UNIVERSITY OF LATVIA

FACULTY OF PHYSICS AND MATHEMATICS

Edgars Nitišs

INVESTIGATIONS OF NONLINEAR OPTICAL ORGANIC GLASS WAVEGUIDES AND THEIR APPLICATIONS

SUMMARY OF DOCTORAL THESIS

Submitted for the Doctoral Degree in Physics

Subfield of Solid State Physics

Scientific Advisor: Dr. Phys. Mārtiņš Rutkis

Riga, 2015

This work was conducted at the Institute of Solid State Physics, University of Latvia, from October 2011 until March 2015.

This work has been supported by the European Social Fund within the project «Support for Doctoral Studies at University of Latvia».

Type of thesis: set of scientific papers in physics, in the subfield of solid state physics.

Scientific supervisor: *Dr. phys.* **Mārtiņš Rutkis**, senior researcher, head of Laboratory of Organic Materials at ISSP, University of Latvia.

Reviewers:

1. *Dr. habil. phys.* **Andris Ozols**, professor, Riga Technical University;
2. *Dr. habil. phys.* **Jānis Spīgulis**, professor, University of Latvia;
3. *Dr. phys.* **Edmunds Tamanis**, professor, Daugavpils University.

The doctoral thesis will be defended at a public session of the Specialized Doctoral Committee of Physics, Astronomy and Mechanics of University of Latvia on 27th of August, 2015 in the conference hall of the Institute of Solid State Physics at 8 Kengaraga Street, Riga.

The doctoral thesis and its summary are available at the Library of the University of Latvia, 19 Raina Blvd., Riga.

Chairman of the Specialized Doctoral Committee of Physics, Astronomy and Mechanics, University of Latvia *Dr.habil.phys.* **Linards Skuja**.

Secretary of the Specialized Doctoral Committee **Laureta Buševica**

ISBN 978-9934-18-028-6

Abstract

The development of information and telecommunication technology rests upon an ever-increasing speed of information processing and transfer. Nonlinear organic materials have been shown to be appealing candidates for the mentioned technologies for the development of optoelectronic and photonic devices. Currently a considerable effort is devoted towards research and characterization of new organic materials for electro-optical applications as well as to development of new types of active waveguide device designs.

In this contribution the author of this thesis presents the results obtained during the implementation of methods for characterization of linear and non-linear optical properties of waveguides, the waveguide poling investigations and the development of a waveguide modulator design.

Keywords: nonlinear optics, organic materials, material characterization, waveguides

Table of Contents

List of abbreviations

$\boldsymbol{A}$ – absorption coefficient
AC – alternating current
ATR – attenuated total reflection
BPM – beam propagation method
$\boldsymbol{C}$ – concentration
CAMFR – CAvity Modelling Framework
CMOS – complementary metal–oxide–semiconductor
$\boldsymbol{d_{iik}}$ – NLO coefficient
DC – direct current
DMABI – dimethylaminobenzylidene-1,3-indandione
DWDM – dense wavelength division multiplexing
$\boldsymbol{E_i}$ – electric field intensity
EME – eigenmode expansion
EMF – electromagnetic field
EO – electro-optic
FDTD – Finite-Diference Time-Domain
$\boldsymbol{f}$ – frequency
FEM – finite element method
IT – information technology
ITO – indium tin oxyde
$\boldsymbol{k}$ – extinction coefficient
$\boldsymbol{k_B}$ – Boltzmann constant
K-K – Kramers-Kronig
$\boldsymbol{l}$ – waveguide thickness
L – Langevin function
LI – lock-in amplifier
LNB – lithium niobate
MR – multiple internal reflection
MZI – Mach-Zehnder interferometric
$\boldsymbol{n}$ – refractive index
$\boldsymbol{N}$ – complex refractive index
$\boldsymbol{n_{ef}}$ – effective refractive index
NLO – nonlinear-optical
$\boldsymbol{P_i}$ – induced polarization in a material
PMMA – polymethyl methacrylate
PS – polystyrol
PSU – polysulphone
$\boldsymbol{r_{iik}}$ – EO coefficient
SEM – scanning electron microscope
SHG – second harmonic generation
SG – Savitzky-Golay filter
SOI – silicon-on-insulator

SP – Silicon photonics
t – time
T_a – glass transition temperature
TC – thickness change
TDM – time division multiplexing
TM – Teng-Man
TPL – two-photon excitation luminescence
WDM – wavelength division multiplexing
$W_{e.s.}$ – chromophore-chromophore electrostatic interaction energy
Θ – light incidence or propagation angle
α_{ii} – first order molecular polarizability
β_{iik} – second order molecular polarizability
γ – propagation constant
κ_o – wavevector
λ – wavelength
μ_o – dipole moment of a molecule
μ_i – induced dipole moment of a molecule
σ – Fresnel coefficient
$\chi_{ii}^{(1)}$ – first order susceptibility
$\chi_{iik}^{(2)}$ or $\chi^{(2)}$ – second order susceptibility
ζ – splitting angle of the Y-coupler in the MZI modulator
ω – angular frequency
$\langle \cos^3 \vartheta \rangle$ – noncentrosymmetric order parameter

1. Introduction

1.1. Motivation

Over the last couple of decades photonics-related research and industry have been growing rapidly. According to Photonics21 (the European Technology Platform for photonics) Multiannual Strategic Roadmap 2014 – 2020 [1], in the nearest future, photonics will have the main role in the growth of measurement technology and informatics. It ought to overcome limitations of electronics in computers through optical computing as well as to provide cheap and effective solutions for optical communications, sensing etc. The field of information technology (IT) has been benefiting greatly from the development of optical communication technology since the first demonstration of the low loss (20 dB/km at 546 nm) optical fiber 1979 by Kapron, Keck and Maurer [2]. The field of optical communications has been developing exponentially ever since. According to the report provided by Cisco, in 2013 the optical communication networks ensured data transmission rates at approximately 1.6 exabytes per month mainly due to the upload and download of visual content such as videos and images [3]. The same report states that the actual demand for data transmission rate is anticipated to exceed 120 exabytes per month in the year 2017. To meet these requirements, new dedicated data transmission solutions will be necessary. In the device level, the growth in data transmission rate may be obtained either:

- through sharing the bandwidth of a single transmission channel among several users via Wavelength Division Multiplexing (WDM), Time Division Multiplexing (TDM) and other techniques [4]; or
- through increasing the speed and efficiency of the individual electro-optically (EO) active elements of the network.

In the field of multiplexing one of the most perspective techniques for high data rate transmission is the Dense Wavelength Division Multiplexing (DWDM). In the DWDM, each signal in one channel is assigned to a different wavelength. The reason why it is called „dense" is due to the fact that the wavelength of each signal that carries information is located very close to each other. Most common standards now include channel spacing of 100 GHz or 50 GHz, while, a sophisticated 25 GHz DWDM was demonstrated more than a decade ago [5]. Lower channel spacing will require accurate tuning and locking the carrier frequencies [6], which is not a simple task to solve and involves development of new type of devices and materials.

A breakthrough will also have to be achieved in performance of the individual elements of the network. One of the critical elements that determines the data transmission rate in the network is the EO modulator. It uses electrical signal to modulate the light intensity or phase. Such modulation can carry

information over optical fibers in both the long-haul and the short-haul communication networks.

The further illustration of the current trends, achievements and issues in the development of EO modulators will be given on the example of Mach-Zehnder interferometric (MZI) type – modulator. The MZI modulator type devices are widely applied in the field of photonics and are currently employed in the commercially available data transmission devices. A schematic illustration of an MZI modulator is shown in Fig. 1.1. The basic principle of an MZI waveguide modulator is the following. The light is coupled into a waveguide and then split into two arms of the MZI using a Y-shaped splitter. The light travels through both of the arms of MZI and then is coupled in a single waveguide using a Y-shaped coupler. In the waveguide the light interference takes place. The light intensity at the output of the MZI depends on the difference between phases of the light that has travelled through both MZI arms. The light phase variation in one of the arms of waveguide MZI would result in a light intensity change at the output of the MZI waveguide modulator. Such phase variation can be obtained through refractive index alteration. This can be achieved by an EO effect in which the refractive index of a nonlinear-optical (NLO) material varies in response to the applied external electrical field. For EO modulation of light phase, an optically intrinsic material is necessary.

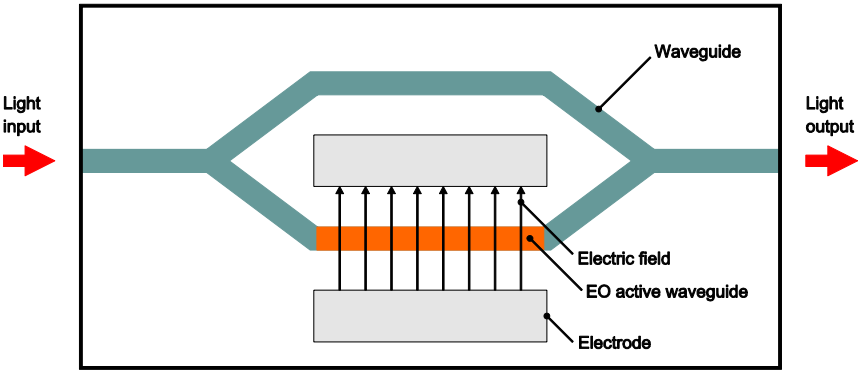

Fig. 1.1. A schematic illustration of an MZI modulator (top view).

For the mentioned application the current standard is to use lithium niobate – $LiNbO_3$ (LNB), which is a nonlinear crystalline material [7]. The light waveguiding structures in the LNB crystal are traditionally formed by a Ti (see Fig. 1.2.A), Zn or MgO ion indifussion or an annealed proton exchange process [8,9]. Such processing allows increasing the refractive index along the desirable light path and thus the waveguide formation. Since the refractive index contrast between the processed and unprocessed parts of LNB is small, the waveguides should be formed at the size of around 10 μm in diameter in order to be able to guide the light [9]. Moreover, the lower the contrast of the

waveguide core (e.g., Ti doped LNB) and cladding (LNB) refractive indices, the higher is light the propagation loss at the waveguide bends [10]. This factor also determines the size of the LNB device.

There are several properties of a LNB waveguide modulator that have made it a long-lasting technology. The LNB modulators are extremely reliable over long periods of time, have stable operation over a wide temperature range, enable the light coupling and propagation loss to be low for visible and infra-red communication wavelengths [11]. However, there are multiple downsides to this material and the associated technology. Firstly, the EO coefficients of the LNB are rather low, but the dielectric constants are high. Due to the low EO coefficients of the LNB, the waveguide device must be made longer – typically up to 10 cm – in order to obtain considerable EO modulation at low voltages [9]. At this modulator size due to the capacitive nature of the modulator it operates as a frequency filter lowering the amplitude of the modulating electric field at high frequencies. Therefore, in order to reach the GHz modulation, the modulator has to be operated in a travelling-wave regime. In this regime the modulating electrical wave travels along with the optical wave in the waveguide causing EO modulation where the waves overlap. Unfortunately, at the GHz frequency range i) the high dielectric constants of the LNB lead to a mismatch between the optical wave and modulating wave to appear and ii) an increasing dielectric and electrode loss begin to dominate the drop in the optical response [7]. Due to the mentioned effects, the LNB based devices have a potential to operate only up to around 100 GHz range [12]. Secondly, the cost of manufacturing and implementation of LNB optical elements in photonics integrated circuits is high mainly due to the difficulty to integrate them with other semiconductor materials.

Nevertheless, LNB modulators are still discussed in the literature. In the last two decades most of the LNB modulator concerned scientific work is aimed towards:

- optimizing the LNB design – finding location of electrodes with respect to the waveguide core, waveguide sizes, etc. for the best device performance [8,13–16];
- finding modulation formats for highest bitrate [17];
- demonstrating new ion-implantation techniques which increase the device efficiency [18]

However, only little increase of the overall LNB modulator performance has been achieved lately. The requirements towards higher speeds and a smaller footprint have made scientists and engineers to look for alternatives to the LNB modulator technology. It is important to note that several good theoretical LNB modulator simulation and bandwidth estimation models have been developed [19–21]. These models are now being successfully applied for EO modulator designs that employ different materials such as barium titanate [22], silicon [23] and polymers [24,25].

Alternative trends in the field of EO waveguide photonics have been emerging lately. One of such is the Silicon Photonics (SP) which is considered to be started by Richard Soref in the late 1980s [26]. The SP was firstly defined to use crystalline silicon for building optical waveguide elements, however, almost all of the group III, IV and V elements and their alloys are being implemented nowadays.

The fundamental element in SP is the silicon waveguide (see Fig. 1.2.B) which is made on a silicon-on-insulator (SOI) wafer by a complementary metal–oxide–semiconductor (CMOS) fabrication process. The SP has many good qualities that suggest that it could become a standard for building devices for optical communications: it is spectrally compatible with the Silica optical fiber used in the optical communication networks, the high refractive index of silicon allows formation of submicron waveguides with small-radius bends thus enabling to build very dense structures on a single chip [27]. Importantly, SP can be processed using the well-established CMOS fabrication process which is the cheapest in terms of price-per-chip manufacturing and allows photonic and electronic integration on a single chip.

However, one of the early problems with the crystalline silicon was its centrosymmetricity (silicon has a cubic lattice structure). This means that originally it does not inherit the EO activity. A solution was again provided by Soref in his work in 1987 where he suggested using the free-charge-carrier-induced electro-absorption and electro-refraction [28]. The index change speed is fast – within the picosecond range [29]. However, high absorption values of doped Silicon as well as high temperature sensitivity have made scientists and engineers to look for alternative EO modulation and switching effects compatible with SP, such as the Franz – Keldysh effect [30], quantum confined Stark effect [31] or EO effect in NLO polymers [32]. From the waveguide preparation cost and integration point of view, the SP is the most mature technology. A single chip along with modulators may also include germanium and silicon photodetectors, multiplexers, light couplers etc. [29].

Another significant drawback to the silicon waveguide is its very high absorption coefficient for wavelengths below 1100 nm, thus the silicon waveguides cannot be used for the visible range. The waveguide operation in the visible range would be relevant for various applications such as inter-connects [33] and photonic spectrometers [34]. One of the currently most popular suggested solutions that would enable the operation of the SP waveguide devices in the visible range would be to use silicon nitride for guiding light (see Fig. 1.2.C.) on the chip [35]. It has the advantage of being transparent in the visible range, being compatible with the CMOS processes, having a high refractive index and being NLO active [36]. However, there are also drawbacks to silicon nitride as a waveguide material. Silicon nitride-based waveguides can reach only limited thickness. Due to intrinsically high film stress of silicon nitride, cracks appear for waveguides that are thicker than 400 nm [37]. Only very recently an improved silicon nitride crack-free waveguide

preparation method has been proposed [38]. Unfortunately, the prepared waveguides still suffer from high light propagation loss due to light scattering.

Possibly one of the cheapest and most effective solutions for creating EO active waveguide devices would be to use NLO organic materials along with silicon. Modulator designs that implement various types of materials, e.g., silicon and polymer, glass and polymer, in the literature are referred to as hybrid designs. The NLO organic materials are particularly interesting for application in the hybrid designs due to their multiple advantageous properties such as low cost, low dielectric constants, high nonlinearity (up to 300 pm/V) and fast response [39,40]. The most straight-forward implementation of a polymer in the SP would be to use the NLO active polymer as a cladding on the silicon waveguides (see Fig. 1.2.D) [41,42]. However, due to the high refractive index of silicon only small part of the guided light will penetrate the EO polymer and "feel" the refractive index change due to the EO effect. To increase the overlap between the guided light and the EO polymer, a design that comprises a silicon slot waveguide filled with the EO polymer has been recently suggested [12,32,43–49]. The high overlap between the light and the EO polymer results in very effective switching – the ON/OFF switching voltage is below 10 V per 1 mm of modulator length and switching is possible at least up to 60 GHz for a modulator with length of a couple of mm [32]. It is worth mentioning that these operation parameters are obtained with a polymer with rather low EO coefficients of 20 pm/V. Clearly the efficiency of the modulator could be increased several times if a highly nonlinear polymer was implemented in the design. There are several drawbacks to the slotted EO active waveguide design that is displayed in Fig 1.2.E. The slot is only a couple of hundred nm wide [46] and, even though it is not emphasized in the literature, filling it with a polymer could be rather tricky due to limited adhesion between the polymer and silicon. Also, the slot should be prepared with high precision in order to have low light propagation loss. Moreover, due to geometry of the waveguide only horizontally polarized light can be guided [49]. This means that if the waveguide application requires coupling of randomly polarized light, additional light coupling loss will take place.

A different approach of preparing hybrid EO active waveguides has been introduced and demonstrated by a group led by Robert A. Norwood [50–54]. The suggested designs employ organically modified sol-gel and polymer waveguides (see Fig. 1.2.F.) that could operate in the visible and infra-red ranges. The light is firstly coupled in a waveguide that is made of a sol-gel material, from which it is afterwards coupled in a NLO active polymer waveguide using a highly efficient adiabatic taper. According to results in the literature at the moment such waveguide designs have the smallest coupling and propagation losses. Waveguide with the principal setup such as demonstrated in Fig. 1.2.F. has been made employing only polymer materials [55–64]. The proposed waveguides could operate a wide optical range

and be very effective. However, the downside of a such design is the cost of preparation which involves multiple lithography and coating steps.

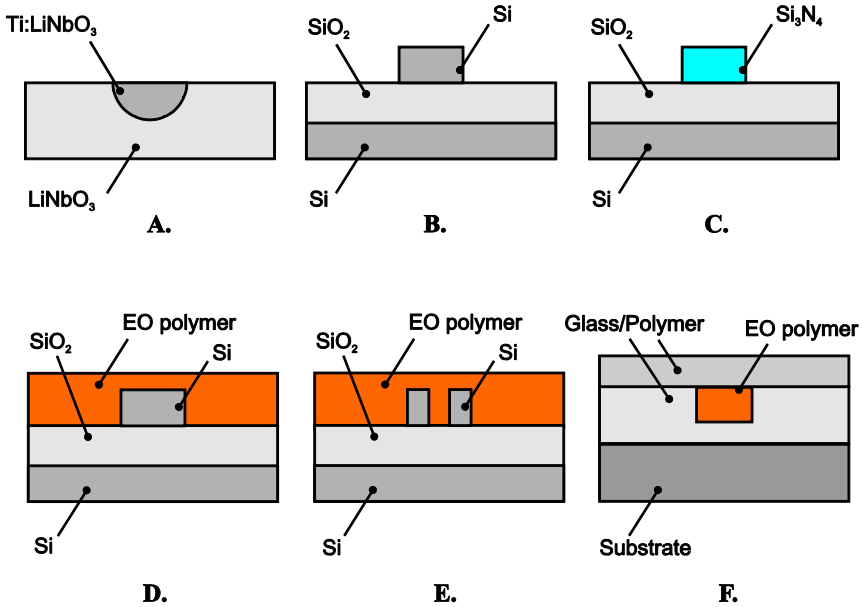

Fig. 1.2. Cross-section of various suggested and employed waveguide designs for application in waveguide modulators. **A.** A Ti:$LiNbO_3$ waveguide in $LiNbO_3$. **B.** A silicon waveguide made on a silicon-on-insulator (SOI) wafer. **C.** An EO silicon nitride waveguide built on a SOI wafer. **D.** A hybrid EO waveguide design comprising silicon and an EO polymer as cladding. **E.** Currently the most effective hybrid silicon and EO polymer design comprising a silicon slot filled with an EO polymer. **F.** Designs that employ EO polymer on glass waveguides or EO polymer on polymer waveguides.

The recent trends clearly outline the fact that EO polymers are considered more and more for application in EO waveguide modulators mainly due to the low cost and high efficiency. Even though one of the first sub-volt EO modulator designs that employed an EO polymer was already presented almost two decades ago [65], the organic EO material has not yet become a standard element in the commercially available EO modulators. There are two main reasons why this has not happened.

Firstly, a major issue with organic EO materials is their thermal and photo-stability [66]. The organic material is thermally stable well below its glass-transition temperature which usually does not exceed 200°C. A commercially available standard EO modulator that comprises an EO organic material would have to comply with the Telcordia standards [67]. The Telcordia standards include the general requirements, such as efficiency,

thermal and mechanical stability, for passive and active waveguide components in EO modulators that are used in conventional communication systems. At the moment the available EO active organic materials do not pass the Telcordia tests. Secondly, the EO organic material based designs that have been proposed and demonstrated up to now are either too expensive or have insufficient efficiency.

Due to the reasons mentioned above, a considerable effort is devoted towards research and characterization of new NLO organic materials as well as towards the development of new type of EO modulator designs. The mentioned tasks are complicated and involve multidisciplinary research in the field of electronics, photonics and chemistry.

The principal and logical levels or steps for the development of an organic material based EO modulator could be the following.

- Molecular engineering – in this step the NLO molecules and their organizations are identified. The recognition of NLO molecules is based on the knowledge of specific molecular features, such as electron donor and acceptor strength, length of the conjugated bridge etc., as well as on the results of Quantum Chemical calculations [68].
- Material synthesis – in this step the NLO material is synthesized.
- Preparation of the material – the synthesized organic NLO material usually (except for some class of crystallic or self-assembling organic materials) requires poling [39]. Poling is a process in which the macroscopic nonlinearity in the material is obtained.
- Investigation of the material – in this step the linear properties (refractive index, absorption) and NLO optical properties (microscopic and macroscopic nonlinearity) of the prepared material are determined.
- Development of the EO device preparation technology – the EO modulator design is identified on grounds of available material preparation technology, material properties and results of numeric simulations.
- Demonstration of the operation – after the EO modulator is prepared, it is tested for stability, switching speeds and voltages.

The results obtained in each of the mentioned steps have crucial effect on the further advancement of the EO polymer modulator technology. Major research groups actively participate and contribute to each of the listed levels.

1.2. Main objective and tasks

The main objective of this PhD thesis was to perform theoretical and experimental investigations of NLO active organic glass waveguides. The following tasks were put forward:

- implement and develop optical methods for characterization of linear properties of EO active organic glass waveguides;
- perform investigations of organic EO active waveguide poling with corona triode;
- implement and develop methods for characterization of non-linear properties of EO polymer waveguides;
- develop a EO waveguide modulator design and preparation technology that comprises organic glass waveguides.

1.3. Scientific novelty

For the first time it is demonstrated that the Abelès matrix formalism can be used for the retrieval of the EO coefficient values from the experimental data obtained by Mach-Zehnder interferometric and Teng-Man methods.

A novel type of hybrid SOI/polymer modulator design and preparation technology is presented. The design and preparation technology is currently pending an EU patent „Electro-optic modulator and method of fabricating same" (EP13196563).

1.4. Author's publications related to this work

[P1] **E. Nitiss**, M. Rutkis, O.Vilitis, Determination of electro-optic coefficient of thin organic films by Mach-Zehnder interferometric method, Latvian Journal of Physics and Technical Sciences 3 (46), 5-14 (2009) **(IF=-, SNIP=0.69)**

[P2] **E. Nitiss**, M. Rutkis, M. Svilans, Effects of the multiple internal reflection and sample thickness changes on determination if electro-optica coefficient values of a polymer film, Lithuanian Journal of Physics 52 (1), 30-38 (2012) **(IF=0.42, SNIP=0.42)**

[P3] **E. Nitiss**, R. Usans, M. Rutkis, Simple method for measuring bilayer system optical parameters, SPIE Proceedings, 8430, 84301C, (2012) **(IF=-, SNIP=0.27)**

[P4] **E. Nitiss**, M. Rutkis, M. Svilans, Electrooptic coefficient measurements by Mach Zender interferometric method: application of Abeles matrix formalism for thin film polymeric sample description, Optics Communications 286, 357-362, (2013) **(IF=1.47, SNIP=1.21)**

[P5] **E. Nitiss**, E. Titavs, K. Kundzins, A. Dementjev, V. Gulbinas, M. Rutkis, Poling Induced Mass Transport in Thin Polymer Films, J. Phys. Chem. B 117, 2812−2819 (2013) **(IF=3.38, SNIP=1.21)**

[P6] **E. Nitiss**, J. Busenbergs, M. Rutkis, Optical propagation loss measurements in electro optical host - guest waveguides, SPIE Proceedings, 8772, 87721L (2013) **(IF=-, SNIP=0.27)**

[P7] **E. Nitiss**, J. Busenbergs, M. Rutkis, Hybrid silicon on insulator/polymer electro-optical intensity modulator operating at 780 nm, J. Opt. Soc. Am. B 31 (10), 2446-2454, (2014) **(IF=1.81, SNIP=1.31)**

[P8] **E. Nitiss**, A. Bundulis, A. Tokmakov, J. Busenbergs, E. Linina, M. Rutkis, Review and comparison of experimental techniques used for determination of thin film electro-optic coefficients, *accepted for publication* Phys. Status Solidi A, 1–13 (2015) / DOI 10.1002/pssa.201532054 **(IF=1.53, SNIP=1.01)**

1.5. Contributions at scientific conferences

[C1] **E. Nitišs**, M. Rutkis, O. Vilītis, Fabrī-Pero etalona veidošanās plāno kārtiņu paraugā un tā ietekme uz EO koeficienta noteikšanu ar MZI metodi, Cietvielu Fizikas Institūta 26. zinātniskā konference, 17. – 19.02, 2010

[C2] **E. Nitiss**, M. Rutkis, O. Vilītis, Corona discharge optimization for nonlinear optical polymer poling, Developments in Optics and Communications, Riga, Latvia, April 23 – 25, 2010

[C3] **E. Nitišs**, M. Rutkis, M. Svilāns, Matricu formālisma pielietošana nosakot plānu organisku kārtiņu EO koeficientu ar Maha Zendera interferometru, Cietvielu Fizikas Institūta 27. zinātniskā konference,. 14. – 16.02, 2011

[C4] **E. Nitišs**, E. Titavs, M. Rutkis, O. Vilītis, Koronas triodes kā NLO polimēru orientēšanas iekārtas voltampēru raksturlīknes, Cietvielu Fizikas Institūta 27. zinātniskā konference,. 14. – 16.02, 2011

[C5] **E. Nitiss**, M. Rutkis, M. Svilāns, Application of Abeles matrix formalism for determination of thin organic film EO coefficients by Mach – Zehnder interferometer, Developments in Optics and Communications, Riga, Latvia, April 28 – 30, 2011

[C6] **E. Nitiss**, E. Titavs, M. Rutkis, O. Vilītis, Poling of EO polymers - Corona Discharge Process Optimization, 12th International Conference Electronic and Related Properties of Organic Systems (ERPOS-12), Vilnius, July 11-13, 2011

[C7] **E. Nitiss**, M. Rutkis, M. Svilāns, Influence Of Multiple Internal Reflection And Sample Thickness Change Effects On Determination Of Polymer Film EO Coefficients Using MZI Technique, Advanced Optical Materials, Vilnius, August 28 – 31, 2011

[C8] **E. Nitiss**, M. Rutkis, Basic principles of EO polymer waveguide modulator development, International Young Scientist Conference "Developments in Optics and Communications 2012", Riga, Latvia, April 12-14, 2012

[C9] **E. Nitiss**, J. Busenbergs, M. Rutkis, Optical propagation loss measurements in electro optical host - guest waveguides, SPIE Optics+Optoelectronics, April 15-18, 2012

[C10] **E. Nitiss**, R. Usans, M. Rutkis, Simple method for measuring bilayer system optical parameters, SPIE Photonics Europe, Brussels, Belgium, April 16-19, 2012

[C11] **E. Nitiss**, A. Tokmakovs, M. Rutkis, Assessment of material refractive index near absorption band using Kramers-Kronig relations,

International Young Scientist Conference “Developments in Optics and Communications 2013”, Riga, Latvia, April 10-12, 2013

[C12] **E. Nitišs**, M.Rutkis, SOI –polimēru EO modulators, LU CFI 30. zinātniskā konference, Rīga, 19.-21.02, 2014

[C13] **E. Nitiss**, M. Rutkis, „Development of polymer electro optic modulator on silicon-on-insulator platform”, International Young Scientist Conference “Developments in Optics and Communications 2014”, Riga, Latvia, April 9-12, 2014

1.6. Patents

[Pa1] „Poled nonlinear polymeric material” (authors S.Gaidukovs, V.Kampars, M.Rutkis, A.Tokmakovs, **E. Nitiss**) patent No. P-13-93 (Latvia)

[Pa2] “The method for limited area of thin polymer film poling” (authors: Vilitis O., **Nitiss E.**, Rutkis M., patent no. 14755 LR (Latvia)

[Pa3] „Poled nonlinear polymeric material”, S.Gaidukovs, V.Kampars, M.Rutkis, A.Tokmakovs, **E. Nitiss**, EP13195779, 05 December 2013 (Submitted, EU)

[Pa4] „Electro-optic modulator and method of fabricating same”, **E. Nitiss**, M. Rutkis, M. Svilans, EP13196563, 10 December 2013 (Submitted, EU)

1.7. Author’s contribution

The main results of this PhD thesis are described in 8 scientific papers [P1-P8] and presented in international and local conferences [C1-C13]. The author was the corresponding author of published and submitted articles as well as for the conference presentations.

A major part of the considered results were obtained by the author. The author:

- implemented and tested the optical setups used for characterization of linear optical properties;
- implemented and tested the Mach-Zehnder interferometric and Teng-Man method for correct measurement of EO coefficients of organic thin films and developed a numerical solution based on the Abelès matrix formalism for the retrieval of the EO coefficient values from the experimental data obtained by Mach-Zehnder interferometric and Teng-Man methods;
- took considerable part in the implementation of the attenuated total reflection technique used for the measurement of thin organic film EO coefficients – developed the optical and electrical setups as well as the methodology for correct interpretation of the EO measurements;
- took considerable part in the thin organic film poling investigations – performed the optical and second harmonic imaging measurements,

performed corona triode device optimization, took part in the analysis and interpretation of the experimental results;

- took considerable part in the development of a hybrid SOI/polymer EO modulator, solely performed the numerical simulations and experimental characterization.

1.8. Preface to further chapters

The further chapters are prepared and arranged according to the logical steps that should be taken in the EO organic material research and the development of an organic material based EO modulator.

The author begins the presentation with the theoretical background necessary for the comprehension of the field of optical waveguiding and nonlinear optics. Only the very essence and key terms of the fields are presented.

Afterwards the author presents the results of linear optical, material poling and nonlinear optical investigations of EO waveguides which are the key elements in the waveguide EO devices. These chapters hold information that is required for correct characterization of used materials as well as for obtaining high quality NLO active organic thin films.

Finally, the author presents a new type of hybrid SOI/polymer EO waveguide modulator. The basic concepts, preparation steps, results of numerical simulations and experimental measurements are presented.

2. Theoretical background

The aim of this chapter is to provide the reader with the information on the basic wave-guiding principles and waveguide parameters that are used for their characterization as well as to give some insight in the origin of optical nonlinearity in organic materials.

2.1. Principles of light waveguiding

An optical waveguide is a structure that is used for confining light and directing its propagation. There are multiple reasons why optical waveguides are used for transferring light signals [69]. Some of the most significant advantageous properties are the following:

- light in the optical waveguides can propagate at long distances without losing energy;
- depending on the optical properties of materials, the cross-section of the optical waveguides can be very small (<1x1 μm), meaning that the waveguide based devices can have a very small footprint;
- the high light confinement in the waveguide provides the possibility to observe enhanced NLO properties of the material.

The total internal reflection effect is used for light confinement in the waveguide. The light refraction and the reflection at the boundary of two different media obey the Snells law which states that the ratio of the sines of the light incidence and refraction angles is reciprocal to the ratio of light refractive index in the two media. The Snell's law can be written in a form

$$n_1 \sin(\theta_1) = n_2 \sin(\theta_2), \tag{2.1}$$

where $\boldsymbol{\theta_1}$ and $\boldsymbol{\theta_2}$ are the angles of incident and refracted beams, respectively, $\boldsymbol{n_1}$ and $\boldsymbol{n_2}$ are the refractive indices of the respective media (see Fig. 2.1). We will assume that the light propagates from a medium with a refractive index $\boldsymbol{n_1}$ into a medium with a refractive index $\boldsymbol{n_2}$ and that the condition $\boldsymbol{n_1}>\boldsymbol{n_2}$ is satisfied. In such case there exists a specific angle called the critical incidence angle $\boldsymbol{\theta_1}=\boldsymbol{\theta_c}$ at which the sine of $\boldsymbol{\theta_2}$ is equal to one. Then from (2.1) the critical incidence angle can be estimated by

$$\theta_c = \arcsin\left(\frac{n_2}{n_1}\right). \tag{2.2}$$

Then, depending on the light incidence angle $\boldsymbol{\theta_1}$, three specific light refraction cases can be outlined: $\boldsymbol{\theta_1}<\boldsymbol{\theta_c}$, $\boldsymbol{\theta_1}=\boldsymbol{\theta_c}$, $\boldsymbol{\theta_1}>\boldsymbol{\theta_c}$. These cases are illustrated in Fig. 2.1. In the first case $\boldsymbol{\theta_1}<\boldsymbol{\theta_c}$ light is simply refracted from the medium 1 into the medium 2. In the second case when $\boldsymbol{\theta_1}=\boldsymbol{\theta_c}$ the refracted beam travels along the interface of the media. If the $\boldsymbol{\theta_1}>\boldsymbol{\theta_c}$, the total internal reflection effect takes place. The characteristic property of this effect is that the efficiency of the reflection is very close to one, thus the optical loss during the reflection is close to zero.

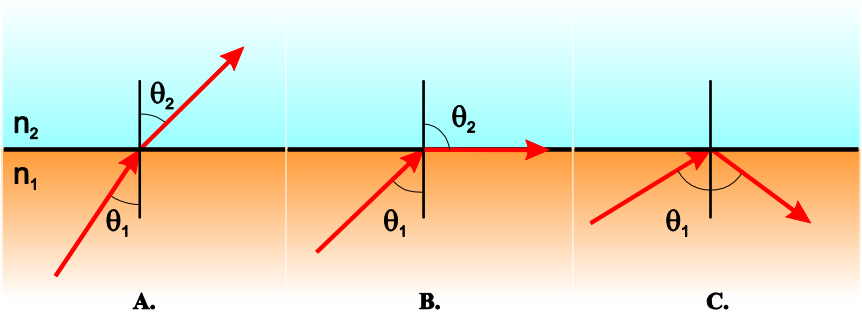

Fig. 2.1. Refraction of light at the boundary of two media with refractive indices n_1 and n_2 so that $n_1 > n_2$. **A.** When the incidence angle θ_1 is smaller than the critical incidence angle θ_c the beam is refracted at $\theta_2 < 90^o$. **B.** When $\theta_1 = \theta_c$ the beam is refracted along the material boundary. **C.** In a case when $\theta_1 > \theta_c$, the beam is internally reflected.

The total internal reflection effect is used for trapping the light in the waveguide. Usually, to illustrate the basic idea the most simple of waveguide structures, which is a planar waveguide, is described. A planar waveguide guides the light only in one dimension and is illustrated in Fig. 2.2. The waveguide core has a refractive index n_1 which must be higher than that of claddings n_2 and n_3 in order for the structure to guide light. We will also assume that $n_2 \leq n_3$. An optical structure can operate as a light waveguide if there is a sufficient refractive index contrast between the core and the lowest refractive index cladding material and the core is sufficiently thick [69].

From the geometrical optics point of view we expect the light to be guided if the incidence angle θ_1 is greater than the critical angle θ_c or $\theta_1 > \theta_c$ (see Fig. 2.2.A). However, as will be shown later, the light is actually guided in the waveguide only at specific resonance θ_1. These guiding conditions are attributed to waveguide modes and can be obtained by solving electromagnetic equations of a guided wave. The electromagnetic wave equations are obtained from Maxwell's equation and can be found in any devoted textbook [69,70]. Only some of the characteristic features and the solution will be outlined in the following paragraphs.

In the waveguide for the propagating light two possible light polarizations have to be considered. In case the propagating light wave has an electric field component in the ***xz*** plane, the waveguide mode is called the transverse magnetic mode. The mode is called the transverse electric mode if the electric field is polarized along the y axis (into the page). Both cases are illustrated in Fig. 2.2.A. For the transverse electric case the electromagnetic wave equation becomes

$$\nabla^2 E_y + \kappa_o^2 n_i^2 E_y = 0, \tag{2.3}$$

where electric field intensity E_y indicates that the light is polarized in the y direction, κ_o is the wavevector in vacuum and is equal to $2\pi/\lambda$, n_i is the refractive index n_1, n_2 or n_3 depending on the location. For the transverse magnetic case the equation (2.3) should be rewritten for the magnetic field value $H_y(x)$. Due to the translation invariance of the problem along z, we expect to look for the solution (2.3) in the form

$$E_y(x,z) = E_y(x)e^{-i\gamma z}, \tag{2.4}$$

where γ is the propagation constant along the z direction and is the eigenvalue of solution of equation (2.3).

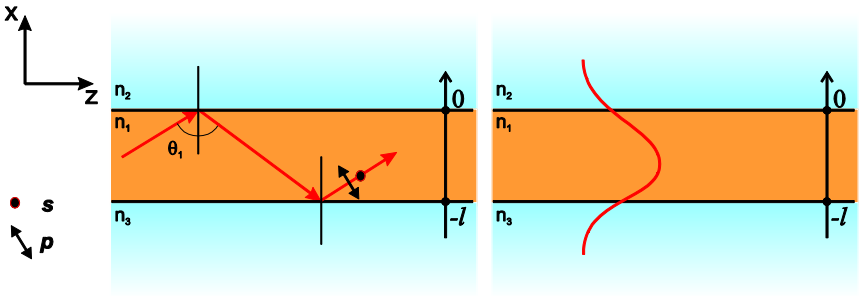

A. **B.**

Fig. 2.2. A planar waveguide consisting of a core with a refractive index n_1 and thickness l and claddings with refractive indices n_2 and n_3 so that $n_2 \leq n_3$. **A.** Geometrical optics representation of light guiding. **B.** Wave optics representation of light guiding – the light intensity also referred to as mode pattern plotted against the z axis, the mode propagates along the z axis.

The solution to (2.3) will give the light electric field E_y distribution over the waveguide. The light intensity distribution in the waveguide (see Fig. 2.2.B) can be obtained by calculating the square of E_y. For the identification of waveguide modes, it is also valuable to use the effective refractive phase index $n_{ef\text{-}p}$ instead of the propagation constant γ. The effective refractive index $n_{ef\text{-}p}$ is more intuitive to operate with. It can be calculated by equation (2.5):

$$n_{ef-p} = \frac{\gamma}{\kappa_o} = n_1 \cos(\Theta_1). \tag{2.5}$$

The reason one would want to operate with $n_{ef\text{-}p}$ is related to the characteristics of the guided mode condition. The guided mode solution exists only to such effective refractive phase index $n_{ef\text{-}p}$ (2.5) which is lower than the refractive index n_1 of the waveguide core and higher than the refractive index of the cladding:

$$\max(n_2; n_3) < n_{ef-p} < n_1. \tag{2.6}$$

Thus only discrete values of $n_{ef\text{-}p}$ in the range defined by (2.6) are allowed.

During the waveguide simulations it should also be taken into account that the light that is coupled into the waveguide has a certain bandwidth. Consequently, to characterize the waveguide modes, the effective refractive group index $n_{ef\text{-}g}$ has to be used instead of the effective refractive phase index $n_{ef\text{-}p}$ [71]. The $n_{ef\text{-}g}$ is a function of $n_{ef\text{-}p}$ and can be calculated by equation (2.7):

$$n_{ef-g} = n_{ef-f} - \lambda \frac{\partial n_{ef-f}}{\partial \lambda}. \quad (2.7)$$

The $n_{ef\text{-}g}$ takes into account the dispersion of the waveguide. It should be noted that $n_{ef\text{-}g} \approx n_{ef\text{-}p}$ for the first modes (modes with the highest $n_{ef\text{-}p}$) of a multimode waveguide if the refractive index of the waveguide core material $n(\lambda)$=const. However, for very small single mode waveguides the difference between group and phase indices can become significant [72]. To facilitate the reading the effective refractive group index $n_{ef\text{-}g}$ of the guiding mode is referred to as the effective refractive index n_{ef}.

The solution to waveguiding problem (2.3) for a simple slab waveguide can be found by solving transcendental equations graphically or numerically. Analytic solutions for two-dimensional waveguides are based on rough approximations, thus are usually solved numerically by finite element methods [69].

2.2. Rectangular waveguides

In previous paragraphs some of the most important parameters used for characterization of the waveguiding condition were shown. The actual integrated optics devices (see Fig. 1.2.) employ waveguides such as buried waveguides, rib waveguides, ridge waveguides and others that confine light in two dimensions [73]. Usually, before developing an integrated optical waveguide device, analytical and numerical simulations are performed in order to solve packaging issues, find optimal parameters for maximal device efficiency etc [72]. Such nontrivial tasks involve calculating the effective refractive index, mode shape and light propagation characteristics such as propagation loss. In the following paragraphs the main tools for performing waveguide and waveguide device simulations that have been used in this work will be briefly described.

2.2.1. Mode solvers

For finding the effective group indices and the shapes of the guiding modes in rectangular waveguides, devoted mode solving tools or mode solvers are used. The mode solving approaches are of different complexity and capabilities, but essentially can be divided into two principal groups.

In the first approach analytic solutions of the modes are used. The first analytic solutions to the rectangular waveguide problem were introduced by Marcatilli [74], however, the method provides precise results only for the first modes of a multimode waveguide (a waveguide that supports multiple modes). Currently the effective index method (EIM) is used as the main analytic tool for

waveguide mode calculations. The EIM was developed by Hocker and Burns in the late 70's [75]. This method allows splitting a two dimensional rectangular waveguide problem into several one dimensional slab waveguide problems which can be easily solved analytically. The EIM works very well for simple geometries, but can introduce errors at the order of couple percent for the effective index and the mode shape of the lowest effective index modes of rib or ridge waveguides [71].

The second principal approach for finding waveguide mode parameters is to use numerical finite element or finite difference eigenvalue solvers that solve Maxwell's equations in a waveguide that is mapped with a cross-sectional mesh [76]. Devoted numerical eigenvalue solvers have shown to provide very low errors and can be used for arbitrary shaped waveguides [77]. Unfortunately, the development and implementation of such numeric eigenvalue solvers can be quite complex and time consuming and, therefore, a common praxis is to use commercial software such as MODE Solutions from Lumerical [78] or Comsol Multiphysics from Comsol [79]. In this thesis for mode solutions of two dimensional waveguide problems the author has used the Electromagnetic Field Module (EFM) which is a part of Comsol Multiphysics. It not only allows one to estimate the mode shapes and effective refractive indices $\boldsymbol{n_{ef}}$, but also to calculate impedances and static electric field distributions if relevant. These additional possibilities are particularly important if numerical EO device optimization is performed.

2.2.2. Propagation solvers

Light propagation simulations are performed within the design flow of waveguide photonics devices. It is important that the device operation and efficiency is estimated theoretically before it is built. For the waveguide devices parameters such as waveguide mode propagations loss, cross-talk and coupling efficiency are calculated by propagation solvers which are mainly numerical. Wide variety of solvers e.g. beam propagation method (BPM), Finite-Diference Time-Domain (FDTD) method, eigenmode expansion (EME) method and others have been implemented, compared and described in literature [80,81]. In this thesis the author has used two different tools for light propagation calculations.

The first tool is the CAvity Modelling Framework (CAMFR) developed by Bienstmann and coworkers [82]. The CAMFR employs EME method which is profoundly described elsewhere [81]. The very basic principle of EME is to use the superposition of a finite number forward and backward eigenmodes (complete basis set) of the waveguide to simulate the light propagation. Such set is defined for each of the invariant elements and the loss is then calculated from the scattering matrices of each element. The CAMFR is run via Python scripts and can be downloaded free of charge at CAMFR homepage [83].

The other tool that was employed for propagation simulations was the EFM of Comsol Multiphysics. The EFM employs a vectorial FEM for calculating meshed optical structures. Depending on the optical element, whether it is a waveguide splitter, Bragg grating or other, either CAMFR of Comsol Multiphysics will be used. CAMFR is better for long invariant and repeating optical structures. On the other hand, the EFM of Comsol Multiphysics allows simple implementation of simulations of irregular and variant structures. Unfortunately, such simulations are more time consuming since usually fine calculation mesh is required.

2.3. Microscopic and macroscopic nonlinearity

As mentioned in the introduction part of this thesis, the waveguides should also be NLO active. In the following paragraphs the origin of optical nonlinearity in materials as well as NLO effects will be shortly discussed.

For the characterization of response of the material to the incident light usually the electric dipole and light interaction model is used. Within this model the light polarizes the molecule. At the microscopic (molecular) level the induced dipole moment $\boldsymbol{\mu_i(\omega)}$ which is a function of the frequency $\boldsymbol{\omega}$ of the incident light with an amplitude $\boldsymbol{E_j(\omega)}$ can be described as:

$$\mu_i(\omega) = \sum_j \alpha_{ij}(\omega) E_j(\omega), \tag{2.8}$$

where $\boldsymbol{\alpha_{ij}(\omega)}$ is the linear molecular polarizability tensor and indices $\boldsymbol{i,j}$=1, 2, 3 denote the vector and tensor components of the electric field and linear molecular polarizability tensor, respectively. The values of tensor components depend on the symmetry of the molecule. For example, in case the molecule is isotropic, then the off-axis components ($\boldsymbol{i \neq j}$) are zero [84].

For high intensity light, such as laser light, the response of the molecule is no longer linear. Therefore the equation (2.8) should be supplemented with higher order nonlinear terms. This is usually done in the following form:

$$\mu_i(\omega) = \sum_j \alpha_{ij}(\omega) E_j(\omega) + \sum_{ij} \beta_{ijk}(\omega, \omega_1, \omega_2) E_j(\omega_1) E_k(\omega_2), \tag{2.9}$$

where $\boldsymbol{\beta_{iik}}$ is the second order molecular polarizability and is a third rank tensor, $\boldsymbol{\omega_1}$ and $\boldsymbol{\omega_2}$ are the applied field frequencies and $\boldsymbol{\omega=\omega_1+\omega_2}$. As a result of nonlinear polarization, it is possible to observe various interesting NLO effects such as second harmonic generation (SHG) – the molecule emits a photon with twice the frequency of incident photons, Pockels effect – change of the refractive index of the material in electric field – and others. Most of the NLO effects start to appear at the electric field intensities in the range of 10^3-10^4 V/cm [85]. The frequencies in the brackets of $\boldsymbol{\beta_{iik}}$ in (2.9) are employed to emphasize the energy conservation in the process. The same frequencies in the brackets can also be used to denote the physical process taking place. Some of the characteristic second order processes and their designations can be found in table 2.1.

Table 2.1. Some characteristic second order processes and their designation [86]

ω	ω_1	ω_2	**Process**
$\omega_1 + \omega_2$	ω_1	ω_2	Up-Conversion
$\omega_1 - \omega_2$	ω_1	$-\omega_2$	Down-Conversion
0	ω	$-\omega$	Optical Rectification
2ω	ω	ω	Frequency Doubling / Second Harmonic Generation
ω	0	ω	Pockels effect

In NLO experiments, such as SHG, usually the macroscopic nonlinearity of the material is observed. The macroscopic nonlinearity of the material can be described using the same concept as for a single molecule. The macroscopic NLO response is governed by the induced polarization $\boldsymbol{P_i}$ in the material. Taking into account the nonlinearity up to the second order, the $\boldsymbol{P_i}$ can be written as

$$P_i(\omega) = \sum_j \chi_{ij}^{(1)}(\omega)E_j(\omega) + \sum_{ij} \chi_{ijk}^{(2)}(\omega, \omega_1, \omega_2)E_j(\omega_1)E_k(\omega_2), \quad (2.10)$$

where $\boldsymbol{\chi_{ii}^{(1)}}$ and $\boldsymbol{\chi_{iik}^{(2)}}$ are the first and second order susceptibilities. Similarly as for a single molecule, the higher even order effects can be observed only if the system is noncentrosymmetric. This condition is easily understood if we look at the induced polarization by an electromagnetic wave. Assuming we have a centrosymmetric system and leaving out the first order susceptibility and losing the indices we can write that

$$P(t) = \chi^{(2)}E^2(t), \quad (2.11)$$

where the electric field intensity varies harmonically

$$E(t) \sim cos(\omega t). \quad (2.12)$$

In case the sign of the incident field amplitude is changed, then we expect to have

$$-P(t) = \chi^{(2)}\big(-E(t)\big)^2 = \chi^{(2)}E^2(t). \quad (2.13)$$

The (2.13) can only be true if the $\boldsymbol{\chi^{(2)}}$=0. Thus a noncentrosymmetric NLO material consists of molecules that possess the second order molecular polarizability and that are not aligned randomly. To obtain a noncentrosymmetric condition in an organic material, it is poled in a static electric field at elevated temperatures. The exception is self-assembling organic materials or organic crystals, which inherit material nonlinearity during preparation [87,88]. We are particularly concerned with the quantities $\boldsymbol{\beta_{iik}}$ and $\boldsymbol{\chi_{iik}^{(2)}}$ and how they relate in a NLO active organic material. If the material is composed of NLO active molecules, also referred to as chromophores, at a concentration $\boldsymbol{C}$, then it is correct to expect that the macroscopic nonlinearity will be the sum of microscopic nonlinearities. For estimation of the second order nonlinearity of the material, we can use the following approximation

$$\chi^{(2)} = C\beta_{\mu}\langle cos^3\vartheta\rangle, \tag{2.14}$$

where $\langle cos^3\vartheta\rangle$ is the noncentrosymmetric order parameter and β_{μ} is the molecular second order polarizability projection on the dipole moment of the NLO active molecule [89]. It is important to note that the noncentrosymmetric order parameter depends also on the chromophore concentration C and dipole moment μ_o of the chromophores. The order parameter, according to an analytic approximation [90], can be expressed as

$$\langle cos^3\vartheta\rangle = \frac{\mu E_p}{5kT}\left[1 - L^2\left(\frac{W_{e.s.}}{kT}\right)\right], \tag{2.15}$$

where E_p is the poling field, T – poling temperature, k_B – Boltzmann constant, μ_o – dipole moment of the molecule, L – Langevin function, $W_{e.s.}$ – chromophore-chromophore electrostatic energy. The relation (2.15) may be divided into two parts. The first part, $\mu_o E/5kT$ describes the order parameter as a function of poling ($\mu_o E$) and thermal depolarization (kT). As can be seen from (2.15), it is desirable to have the poling energy ($\mu_o E$) as high as possible for maximal ordering. This obviously can be achieved by increasing the poling field E_p strength. The second part of (2.15) $(1\text{-}L^2(W_{e.s.}/kT))$ characterizes the dipole-dipole interactions of the NLO molecules in the material, which tend to reduce the order parameter due to repulsion of dipoles oriented in the same direction. The dipole-dipole interaction is also responsible for the reduction of the NLO efficiency by stimulating formation of centro-symmetric NLO inactive aggregates, especially in guest-host systems where chromophores can move within a matrix.

Some molecule related characteristics and their effect on the second order response should be outlined:

- all higher even order polarizabilities are zero for a centrosymmetric molecules [89]. Usually, the molecule that possesses the higher order molecular polarizabilities consists of three parts – electron donor group, electron acceptor group and a conjugated bridge that separates donor and acceptor groups [39];
- the second order response depends on the resonance frequency ω_r of the molecule and the frequency ω of the incident light [89]. The two-level model gives the following proportionality for the off-resonance case [91]:

$$\chi^{(2)}(\omega) \sim \frac{\omega_r^2}{(\omega_r^2 - 4\omega^2)(\omega_r^2 - \omega^2)^2}. \tag{2.16}$$

2.4. Second order NLO effects

The equation (2.10) can be used for characterizing second order response of the material. For the sake of clarity some frequency arguments will be suppressed in the further equations. As can be seen from (2.10), the non-linear polarization in a simple form can be written as

$$P_i = \sum_{ij} \chi_{ijk}^{(2)} E_j E_k. \tag{2.17}$$

Due to Kleinman's symmetry the $\chi_{iik}^{(2)}$ can be reduced from a 3x3x3 tensor to a 3x6 tensor which simplifies the usage of (2.17) [85]. The indices "***jk***" are replaced by "***h***" so that

$$h = \begin{Bmatrix} 1 & j,k = 1,1 \\ 2 & j,k = 2,2 \\ 3 & j,k = 3,3 \\ 4 & j,k = 2,3;3,2 \\ 5 & j,k = 1,3;3,1 \\ 6 & j,k = 1,2;2,1 \end{Bmatrix}. \tag{2.18}$$

If the material is characterized using SHG measurements, usually the second order susceptibility $\boldsymbol{\chi_{iik}^{(2)}}$ is substituted by $\boldsymbol{d_{iik}}$ where the coefficients in the tensor are called the NLO coefficients. For a poled organic material which belongs to point group symmetry of $\boldsymbol{mm\infty}$, the nonlinear polarization can be calculated from (2.19) [92]

$$\begin{pmatrix} P_1 \\ P_1 \\ P_1 \end{pmatrix} = \begin{pmatrix} 0 & 0 & 0 & 0 & d_{31} & 0 \\ 0 & 0 & 0 & d_{31} & 0 & 0 \\ d_{31} & d_{31} & d_{33} & 0 & 0 & 0 \end{pmatrix} \begin{pmatrix} E_1^2 \\ E_2^2 \\ E_3^2 \\ 2E_2^2E_3^2 \\ 2E_1^2E_3^2 \\ 2E_1^2E_2^2 \end{pmatrix}. \tag{2.19}$$

As can be seen from (2.19), for NLO active organic material characterization only two independent tensor elements $\boldsymbol{d_{31}}$ and $\boldsymbol{d_{33}}$ have to be used.

Similar notation is used to characterize the Pockels effect which is also called the linear EO effect. The Pockels effect is responsible for the change of the material refractive index with applied electric field. This is a second order NLO effect which can be observed in noncentrosymmetric media. The change of the refractive index can be written as

$$\Delta\left(\frac{1}{n^2}\right)_{ij} = \sum_k r_{ijk} E_k, \tag{2.20}$$

where $\boldsymbol{r_{iik}}$ is the EO coefficient tensor. Applying the same symmetry rules and now substituting indices "***ij***" with "***h***" as in (2.18), we get that the refractive index change for a material which belongs to the point group symmetry of $\boldsymbol{mm\infty}$ can be expressed as:

$$\begin{pmatrix} \Delta\left(\frac{1}{n^2}\right)_1 \\ \Delta\left(\frac{1}{n^2}\right)_2 \\ \Delta\left(\frac{1}{n^2}\right)_3 \\ \Delta\left(\frac{1}{n^2}\right)_4 \\ \Delta\left(\frac{1}{n^2}\right)_5 \\ \Delta\left(\frac{1}{n^2}\right)_6 \end{pmatrix} = \begin{pmatrix} 0 & 0 & r_{13} \\ 0 & 0 & r_{13} \\ 0 & 0 & r_{33} \\ 0 & r_{13} & 0 \\ r_{13} & 0 & 0 \\ 0 & 0 & 0 \end{pmatrix} \begin{pmatrix} E_1 \\ E_2 \\ E_3 \end{pmatrix}. \quad (2.21)$$

Similarly as for the SHG effect, there are only two independent tensor elements r_{13} and r_{33} that should be determined for characterization of EO properties of the material. The EO and SHG matrices appear to be very similar for the same point group symmetry. Indeed, the magnitudes of the matrices are also related and possess proportionality; however, the relationship does not agree precisely because the measurement conditions are different. Usually, the linear EO effect is observed at frequencies which are much lower than those of SHG. The relevant relationship between the coefficient of EO and NLO tensors is the following ratio

$$\frac{d_{33}}{d_{31}} = \frac{r_{33}}{r_{13}}. \quad (2.22)$$

A simple approximation of the order parameter in the poled polymer materials suggest that for films poled at low electric fields the r_{33}/r_{13} ratio should be in the range from 1 to 3 [93]. However, deviations from the isotropic model have been registered experimentally, suggesting that this ratio could be up to the value of 6 [94,95].

2.5. Theoretical background: Summary

The total internal reflection effect is used for trapping light in the waveguide. The waveguide consists of a core and claddings where the core material has a higher refractive index than those of cladding materials. The light waveguiding is a resonance process – the light can be guided at certain conditions which are characterized by optical modes. The resonance conditions can be estimated by analytical and numerical methods. In order for the waveguide to be used in the EO waveguide devices, it must not only be able to guide light, but also to be optically nonlinear. The optical nonlinearity of the materials is characterized by the second order susceptibility tensor which for EO effect is denoted as EO coefficient r_{ij}, but for SHG effect – as NLO coefficient d_{ij} tensor. Poled NLO polymers belong to the point group symmetry of $mm\infty$ which means that in the NLO organic materials there are only two independent elements in a susceptibility tensor.

3. Characterization of linear optical properties

In the waveguide device fabrication process it is important to know the linear optical properties of the waveguides used in the design. The main linear optical properties of the waveguides are the waveguide thickness, waveguide material refractive index and the light optical propagation loss in the waveguide. All of these parameters determine the operation of the waveguide device and the validity for the intended application. For example, an incorrect estimation of the thickness and the refractive index may lead to significant errors of the estimated nonlinearity of the waveguide material and thus incorrect evaluation of the NLO efficiency of the device [96].

Various methods for the characterization of linear optical properties of waveguides have been suggested and described in the literature. Commonly optical methods such as single wavelength or spectral ellipsometry [97–99], spectral interferometry [100], and spectral reflectometry [101–103], are used for the evaluation of waveguide refractive index and thickness. With most of the mentioned methods it is possible to obtain the product of the refractive index and thickness with a very high precision, even for samples with thickness of a couple of tens of nanometers. However, most of them employ sophisticated functions for transmission or reflection data approximation. Moreover, most of the mentioned techniques cannot be used to estimate linear optical parameters of bilayer waveguide, e.g., waveguide with a core layer and a cladding layer. In the following paragraphs the author of this thesis demonstrates an implemented simple spectral reflectometry technique that can be used for estimations of thicknesses and refractive indices of a bilayer waveguide. The method is based on interference fringe separation and can be used for optical parameters in the low absorbance part of the waveguides.

Unfortunately, the previously described optical methods are usually insufficiently powerful for the direct refractive index measurement near the absorption band due to the fact that most of the light is absorbed in the material. One of the solutions for the evaluation of the refractive index near and at the absorption maxima of the material would be to apply the Kramers-Kronig (K-K) relations [104–107]. The K-K relations can be used to calculate the real part of a refractive index by integrating the imaginary part – extinction coefficient – of the material. The great advantages of this method, besides the fact that it can be used for the measurement of refractive index near the absorption band, is that it is a noncontact method and it does not require sophisticated experimental tools. The K-K transforms have also been implemented in the workflow of EO material characterization.

In addition to the methods that can be applied for the determination of refractive indices and thicknesses of waveguides, the author of this thesis has also implemented a method for investigation of the light propagation loss in the waveguide. As noted in the previous paragraphs, the light propagation loss is one of the parameters used for the characterization of a waveguide device.

In the succeeding paragraphs the following implemented methods will be discussed:

- spectral reflectometry – a noncontact method for thickness and refractive index measurements of a single or bilayer waveguide [P3];
- the K-K relations used for determination of the waveguide refractive index from the simple extinction coefficient measurements of a waveguide [C11];
- the travelling fiber method – a method used to determine the light propagation loss in the waveguide [P6].

3.1. Spectral reflectometry

The implemented spectral reflectometry method for measuring bilayer system optical parameters in the low absorbance part of the sample transmittance or reflectance spectrum has been described by the author in [P3].

Even though, similar spectral measurement based methods for single layer optical parameters have been discussed earlier in the literature [108,109], the author extends the approach for characterization of bilayer systems.

The reflection spectrometry is based on collecting reflected light from a multi-interface system and can be used to determine the optical path length of certain layers in the system. Let us assume that light $\boldsymbol{I_o}$ is incident on the sample – a simple waveguide on a glass substrate. The reflected and transmitted light intensity $\boldsymbol{I_r}$ and $\boldsymbol{I_r}$ will depend on the refractive index of each medium and the thickness of the thin layers in which multiple internal reflections can take place. In such case fringes can be noticed in the reflected spectrum. The period of these fringes is determined by the optical path length of the thin film which is a product of the refractive index of the waveguide $\boldsymbol{n_1}$ and thickness $\boldsymbol{l}$. The reflectivity $\boldsymbol{R}$, which is the ratio of reflected light $\boldsymbol{I_r}$ and incident light $\boldsymbol{I_o}$ intensities, of the non-absorbing thin film at zero light incidence angle can be calculated by

$$\frac{I_r}{I_o} = R = \left|\frac{\sigma_{12}+\sigma_{23}\exp(-2i\delta)}{1+\sigma_{12}\sigma_{23}\exp(-2i\delta)}\right|^2. \tag{3.1}$$

where

$$\delta = \frac{2\pi n_1 l}{\lambda}, \tag{3.2}$$

and $\boldsymbol{\sigma_{12}}$ and $\boldsymbol{\sigma_{23}}$ are the Fresnel coefficients [110] of the air – thin film and thin film – substrate interfaces respectively, and $\boldsymbol{\lambda}$ – the wavelength.

To demonstrate the characteristics of this light interference effect the spectral reflectivity of a waveguide on a glass substrate will be discussed. The reflectivity of a waveguide on a glass substrate according to (3.1) is plotted in Fig. 3.1. Three particular cases are illustrated in this graph. In the first case a 1 μm thin waveguide is on a substrate with refractive index 1.45, in the second – on a substrate with refractive index 1.5 and in the third case – on a substrate

with refractive index 1.6. It is important to note that therein an approximation for the refractive indices is used – the dispersion of the substrate and the thin film is neglected, meaning that the refractive index of substrate and the thin film is constant over the plotted wavelength range from 400 nm to 900 nm. Nevertheless, the plot illustrates some important properties of the reflected light spectra. Firstly, it can be noticed that fringes appear and that the extreme points in the reflected light spectra are fixed and independent of substrate refractive index. The location of extreme points is determined only by the thickness and the refractive index of the waveguide. Secondly, the higher the refractive index contrast of the substrate and the thin film, the higher is the amplitude of the interference fringes. From these observations it can be concluded that the dispersion of substrate material would cause the amplitude of the fringes to vary across the reflected light spectra, but would not affect the location of the interference extreme points.

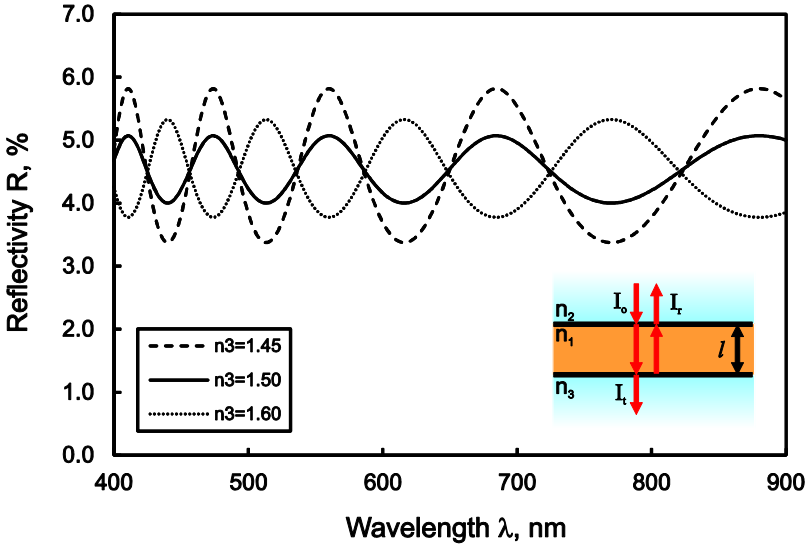

Fig. 3.1. The reflectivity of a thin waveguide with a refractive index of n_1=1.54 on a glass substrate with a refractive index n_3. The third medium is air with a refractive index n_2=1. Three particular cases are illustrated: in the first case a 1 μm thin film is on a substrate with refractive index 1.45 (dashed line), in the second – on a substrate with a refractive index 1.5 (solid line) and in the third case – on a substrate with a refractive index 1.6 (dotted line).

In the demonstrated technique the refractive index and the thickness of the waveguide is determined from the location of extreme points in the reflected spectra. In the paper [P3] a new penalty parameter for finding the refractive indices and thicknesses of the layers is introduced. The penalty

parameter is the standard deviation of calculated thicknesses at wavelengths corresponding to the extreme points. For the thin film refractive index approximation point-by-point and Sellmeier dispersion relation were used.

The experimental setup consisted of a light source, optical fiber probe, a sample and a spectrometer. The light from a light source is transmitted through a reflection probe to the sample. The light reflected from the sample is then collected and transmitted to a spectrometer. As reported in [P3], the implemented technique was tested on a single layer and bilayer waveguides showing good results of thickness and refractive index estimates. Only results on obtained for a bilayer system will be discussed in the following paragraphs.

The test samples were prepared following the steps depicted in Fig. 3.2. An indium tin oxide (ITO) covered glass (see Fig. 3.2.A) was used as a substrate. The thickness of the ITO layer is around 60 nm, but its refractive index is around 2 in the visible range. As noted previously, it is suggested to have refractive index contrast materials in the sample in order to have higher amplitudes of interference fringes. A polymer thin film was spin-coated from a chloroform solution onto the ITO covered glass slide (see Fig. 3.2.B and 3.2.C). The polymer used was a host-guest material consisting of a dimethylaminobenzylidene-1,3-indandione (DMABI [111]) chromophores as guests in polymethyl methacrylate (PMMA) (Sigma-Aldrich) doped at 10%wt. Henceforth, such host-guest material will be referred to as DMABI+PMMA 10%wt. The thickness of the spin-coated samples is typically around 1 to 2 μm. The refractive index of DMABI+PMMA 10%wt is 1.54 at 633 nm. Such thin film (see Fig. 3.2.D) can be used as a waveguide. It usually supports multiple modes in the visible wavelength range. A bilayer system was obtained by covering a glass slide carrying a spin-coated polymer film with another ITO covered glass slide. Afterwards both slides were squeezed together in the sample holder creating a system as shown in Fig. 3.2.E. On the micron scale the surface of the polymer sample, especially at slide edges, is rather rough causing the formation of an air gap between the surface of the polymer and second ITO layer thus a bilayer system in the micron scale is created. Such sample structure can be used for polymer poling purposes. In order to estimate the voltage drop on the NLO polymer film, it is very important to know the thickness of the air gap.

The collected spectrum from the prepared bilayer sample is evident in Fig. 3.3. Evidently, the experimentally obtained reflectivity curve is not as smooth as the theoretical one shown in Fig. 3.1. It needs to be filtered to reduce the noise and to be able to extract the wavelengths which correspond to the extreme points in the reflectivity curve. For the collected raw data the Savitzky-Golay smoothing (SG) filter was applied [112,113].

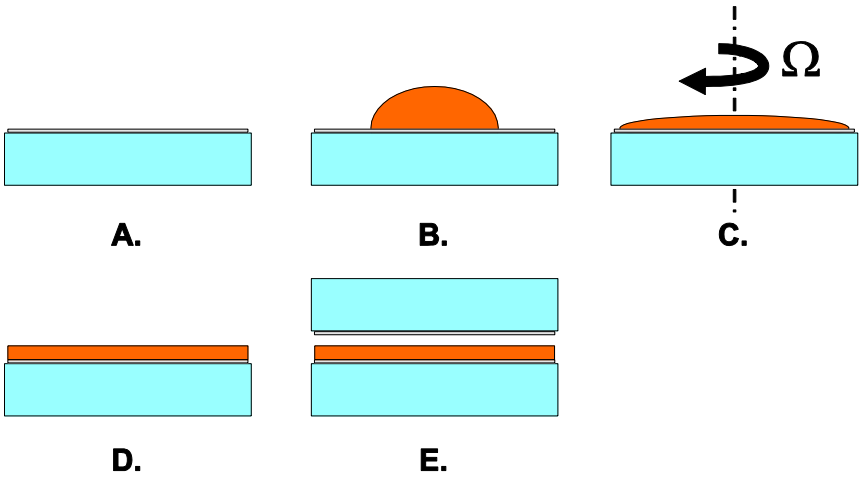

Fig. 3.2. Preparation of a bilayer sample. **A.** An indium tin oxide (ITO) covered glass substrate. **B.** A small amount of chloroform solution is applied onto the ITO covered glass slide. **C.** During the spin-coating process the substrate is rotated at appropriate angular velocity ***Ω*** and the solution is spread over the substrate. **D.** As a result of spin-coating, a thin and smooth polymer film on the ITO covered glass slide is obtained. **E.** A bilayer system in the micron scale is created by covering the polymer carrying ITO covered substrate with another ITO covered substrate.

From the spectrum shown in Fig. 3.3 it is clearly evident that the spectral intensity is governed by interference effects in two layers with different optical path lengths. In the reflected light spectrum the wavelength separation of fringes caused by the thicker layer should be smaller and for the thinner ones – larger. Thus it is assumed that the long period fringes are caused by interference in the thin film, but the short period ones – by the interference in the air gap. The optical parameters for each of the layers can be obtained by separation of the interference fringes.

To extract the interference fringe corresponding multiple internal reflections in the thin film, an SG filter with a 701 points wide window length was applied and a smooth curve referred to as 1st SG filter was obtained. From the filtered data three extreme points were found. The calculated thickness of the thin film was 0.73±0.01 μm using the point by point and 0.91±0.01 μm using the Sellmeier dispersion relation.

If the SG filtered values are subtracted from the raw data, the shorter period interference fringes can be separated. The shorter period interference fringes or the filtered raw data in the spectral range from 710 to 870 nm are shown in the smaller graph in Fig. 3.3. After application of the SG filter of the window length of 101 points (2nd SG filter), the wavelengths corresponding to

the extreme points in the reflected spectra can be found. From these points the optical parameters of the air gap can be calculated giving the gap width of 5.55±0.29 μm when using point by point method and 5.97±0.14 μm when using the Sellmeier dispersion relation in the 710 – 870 nm range.

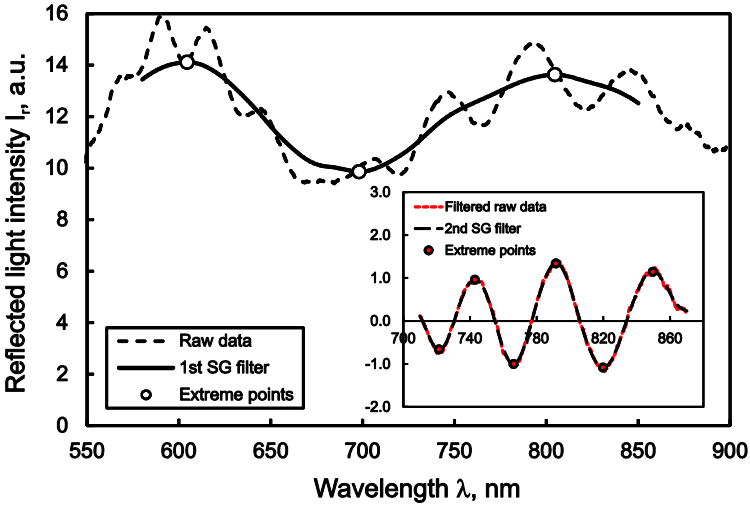

Fig. 3.3. The reflected light spectra from the bilayer sample, filtered data using SG filters and the extreme points from which the thicknesses and refractive indices of layers are obtained.

It is important to note that in order to have interference fringes that can clearly be separated by SG filtering, the layers must have optical path lengths that differ at least a couple of times. The method is limited to be used in the low absorption region of the reflection or transmission spectra.

3.2. Kramers-Kronig relations

As mentioned previously for the evaluation of refractive index near and at the absorption maxima of the material, one would apply the K-K relations. The author of this thesis has implemented the K-K relations for determination of refractive indices of absorbing thin films. The results were reported at an international conference [C11].

In general the K-K relations bind the real and imaginary part of any analytic function ***B*** in the form

$$\mathrm{B} = B_1 + iB_2. \tag{3.3}$$

Physically the $\boldsymbol{B_1}$ and $\boldsymbol{B_2}$ can be the real and imaginary parts of a material response function of a time dependent property [114]. In optics the K-K relations are applied for finding the complex refractive index ***N*** which is an analytical function and can be written as

$$N = n + ik. \tag{3.4}$$

The K-K relations that bind the real and complex parts of the refractive index are in the form

$$n(\omega) = KK\big(k(\omega)\big) + n(\infty) = \frac{2}{\pi}\int_0^{\infty} \frac{\omega' k(\omega) d\omega'}{\omega'^2 - \omega^2} + n(\infty). \tag{3.5}$$

There are only few functions ***k(ω)*** for which the K-K transformations can be performed analytically [115]. Usually the extinction coefficient function ***k(ω)*** has an arbitrary shape and thus numerical integration of the integral (3.5) has to be performed. As obvious from (3.5), there are some limiting factors that should be noticed. Firstly, the integral in (3.5) has a pole at ***ω'=ω*** at which ***n(ω)***$\rightarrow\infty$. Thus integration at the pole frequency should be avoided. Secondly, integration to infinity should be performed according to (3.5) even though the ***k(ω)*** is recorded in a specific range. Integration to infinity can be substituted by an integration in a specific range only if ***k(ω)*** outside the range is zero. Taking into account the mentioned limitations, numeric methods for finding ***n(ω)*** have been implemented [116,117]. According to Ohta and Ishida [118], the integration using Maclaurin's formula might be one of the most efficient methods in terms of obtained precision and the required computer calculation time. The Maclaurin's formula calculates the value of the integral (3.5) by a very simple summation procedure. In the summation the extinction coefficient at every other frequency point is used. Thus the refractive index at specific frequency can be written as

$$n(\omega'_v) = \Delta n(\omega'_v) + n(\infty) = \frac{4}{\pi}\sum_{\omega' u} \frac{(\omega' u+1 - \omega' u)\cdot \omega' u \cdot k(\omega' u)}{\omega'^2_u - \omega'^2_v} + n(\infty). \tag{3.6}$$

The summation by ***u*** in (3.6) is performed at every other data point in order to avoid situation where dominator of (3.6) is zero. The starting point of the summation is chosen such that the situation when ***u***=***v*** is avoided: if ***v*** is odd, then ***u***=2, 4, 6, .., but if ***v*** is even, then ***u***=1, 3, 5, .. .

The implemented numeric K-K transformation was tested for finding the refractive index ***n(λ)*** of DMABI+PMMA 3%wt thin film. From the material under investigation a thin film of thickness of around 1.5 μm was prepared on a glass substrate using the spin-coating method. Using the Metricon 2010 prism coupler the refractive indices of DMABI+PMMA 3%wt at 1064 nm, 632.8 nm and 532 nm were estimated to be $n(\lambda_{1064})$=1.495, $n(\lambda_{632.8})$=1.504 and $n(\lambda_{532})$=1.528. The absorption spectra ***A(λ)*** of the thin film were recorded using a simple transmission configuration comprising a light source, the sample under investigation and a spectrometer. From the absorption spectra the extinction coefficient spectra were calculated using a simple equation

$$k(\lambda) = \frac{A(\lambda)\cdot\lambda}{4\pi}. \tag{3.7}$$

The obtained extinction coefficient from the absorption spectra of DMABI+PMMA 3%wt thin film is shown with a black line in Fig. 3.4.A. In the spectra, a characteristic peak of DMABI+PMMA 3%wt with the resonance

frequency at 490 nm is visible. Unfortunately, the recorded spectrum also holds some contribution from the glass, which has a significant absorption below 400 nm. Some background noise and loss due to reflections is also evident after 500 nm. Even though in absolute units the noise and loss due to reflections is small, it appears impressive due to the fact that the extinction coefficient is in logarithmic units. In order to be able to use the numerical K-K transform for the obtained extinction coefficient ***k(λ)***, the absorption peak characteristic to the material must be extracted. Therefore, a function which is a sum of two Gaussian functions is used to for the approximation of the peak. A least-square fit of ***k(λ)*** in the range of 400 nm to 520 nm with two Gaussian functions was performed. The sum of the two Gaussian functions gives a filtered ***k(λ)*** for which the numeric K-K transform is applied. It is important to note that, according to (3.6), ***n(λ=0)*** must be added to ***Δn(λ)*** obtained from the K-K transform. This means that for correct estimation of ***n(λ)*** from ***k(λ)*** it is necessary to know the refractive index at least at one wavelength in order to fit the ***n(λ=0)*** value.

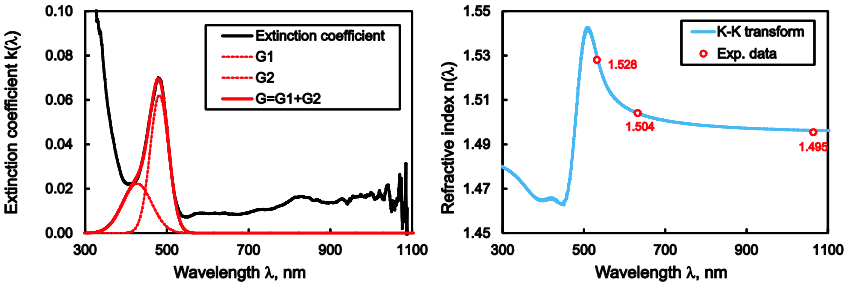

Fig. 3.4. A. The measured extinction coefficient ***k(λ)*** of DMABI+PMMA 3%wt thin film sample (black line), Gaussian approximations G1 and G2 (red dashed lines) used to characterize the absorption peak characteristic to the material and the obtained sum of two Gaussian functions (G=G1+G2). **B.** The refractive index ***n(λ)*** obtained from the numeric K-K transformations (blue line) and the refractive indices of DMABI+PMMA 3%wt at 1064 nm, 632.8 nm and 532 nm obtained by the m-line method (red points) have good agreement.

There are some additional approximations used in this approach. The implemented method does not take into account the loss and interference effects that may appear due to reflections at the interfaces. The mentioned effects may cause errors in the obtained dispersion function ***n(λ)*** [107,119]. To avoid the appearance of interference fringes in the ***k(λ)*** spectra low refractive index contrast layers should be used. In Fig. 3.4.B the refractive index ***n(λ)*** obtained from the numeric K-K transformations as well as refractive indices of DMABI+PMMA 3%wt at 1064 nm, 632.8 nm and 532 nm obtained by the m-line method (*Metricon* 2010 prism coupler) are plotted. Evidently, the

dispersion function ***n(λ)*** has a good agreement with the experimental data points.

3.3. Travelling fiber method

For the development of waveguide devices the optical quality of the waveguide is very important, because it is one of the parameters that determine the overall efficiency of the device. It has been recognized that, in a waveguide EO modulator the light propagation loss should be no more than 1 dB/cm, in order to ensure wide commercial utilization of the device [120]. In other words, only 20 % of power loss per cm is allowed. There are multiple effects that can contribute to the light propagation loss [69]: loss at the waveguide bends; scattering loss – light is scattered, usually at the waveguide core-cladding boundary; absorption loss – light is absorbed in the waveguide core or cladding. The absorption loss is usually governed by the optical properties of the employed core and cladding materials, but the scattering loss occurring at the waveguide boundaries mainly depends on the waveguide preparation technology [121].

There are multiple methods for measuring optical propagation loss in waveguides [122,123]. The most commonly applied is the cut-back method [121,124,125]. In this method, the light is coupled in a waveguide, which is afterwards clipped or cut, thus allowing the transmission of light for waveguide with different lengths to be compared. This method is a destructive measurement method and is usually applied for inorganic materials. The inorganic materials such as LNB and silicon have crystallographic planes and therefore are easy to cut, in contrast to soft organic waveguide.

One can also use nondestructive methods such as multiple prism coupling [126]. In this method multiple prisms are used to simultaneously couple light in and out of the waveguide. The light propagation loss is estimated by moving one of the prisms and monitoring the intensity of the output light. Even though the realization of the method sounds simple, the actual implementation of simultaneous two prism light coupling may be cumbersome.

Another nondestructive method for measuring light propagation loss in a waveguide is the travelling fiber method [126–128]. In this method the light that is scattered at the boundary of the waveguide is collected along the light propagation path. The author has implemented the travelling fiber method for measuring the light propagation loss in polymer waveguides. For detailed description of the method and results, see paper [P6]. Before discussing the advantages and drawbacks of the method, the principles of the implemented method are shortly discussed.

The prism coupling technique was applied for coupling light into planar optical waveguides [123,129]. The principal scheme of the setup is depicted in the left bottom corner of the Fig. 3.5. Full scheme of the experimental setup can be found in [P6]. The incident beam from a laser is coupled through a high

refractive index prism into a planar waveguide. The light can be coupled at incidence angles that correspond to mode resonance angles in the waveguide. As optical mode propagates in the thin film, part of the intensity is scattered at the waveguide boundary. This scattered light is collected using a multimode optical fiber. If it is assumed that the surface roughness and the waveguide inhomogeneity is maintained throughout the light propagation path and that the scattered light intensity is proportional to the light intensity in the waveguide core, then the propagation loss can be estimated.

As an example, the measured scattered light intensity for NLO guest-host polymer DMABI+PMMA 12.5%wt waveguide as a function of light propagation distance is shown in Fig. 3.5. It can be seen that the light intensity decays exponentially as the light propagates through the waveguide. The experimental data do not lie smoothly on the approximation curve and some bumps can be noticed. These are caused by additional scattering elements in the sample such as dust or crystalic phase. The scattering objects are formed during the sample preparation, but should be avoided for a good optical propagation loss measurement. The approximation of the experimental data is also evident in Fig. 3.5 yielding that the optical propagation loss for this particular measurement is 9.6 dB/cm at 632.8 nm.

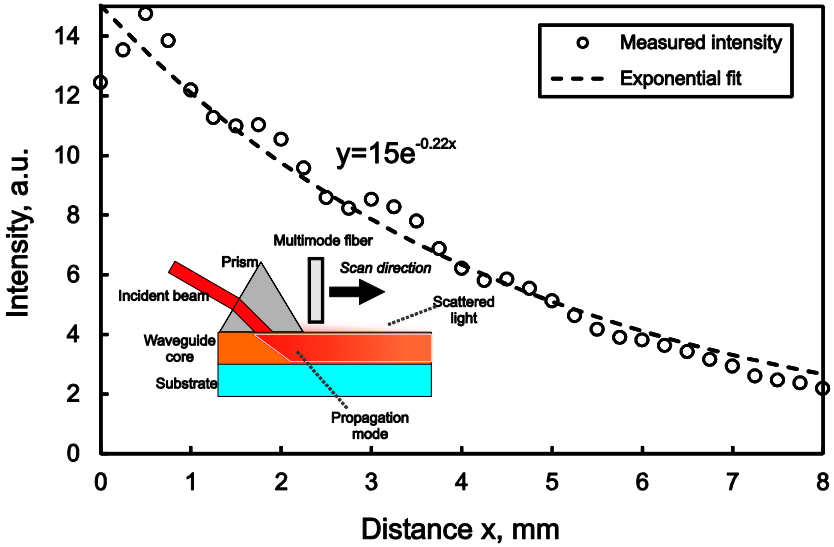

Fig. 3.5. The principal scheme of a light propagation loss measurement by the travelling fiber method (bottom left corner) as well as the measured scattered light intensity as a function of the light propagation length ***x***.

This method possesses multiple commonly known disadvantages which were confirmed by the author of this thesis during the implementation of the

method: the waveguide surface must scatter the light which inevitably causes additional optical loss, it does not work for buried waveguides and it requires precise mechanical operation [130]. The main advantage of this method is the simplicity of execution and, even though an indirect optical loss measurement is performed, it can give good results.

The author used this method for measuring the light propagation loss dependence on the NLO chromophore doping concentration in guest-host polymer waveguides. According to the work conducted by Rutkis and colleagues [111], for doping concentrations below 15%wt the nonlinearity of the waveguide is expected to increase as the concentration is increased. The light propagation loss measurements indicated that only low doping <1.5%wt is allowed in order to have the light propagation loss below 1 dB/cm or 20% loss per cm waveguide length [P6]. The travelling fiber method was also used to estimate how the thickness of SiO2 cladding influences the light propagation loss of planar DMABI+polysulphone (PSU) waveguides on an oxidized silicon wafer [P7]. Based on these results, a new type of hybrid polymer-SOI modulator design was suggested (see section 6).

3.4. Characterization of linear optical properties: Summary

The author has implemented three methods for characterizing the waveguide refractive index and thickness as well as the optical propagation loss in optical waveguides. The approaches allow characterization of both multilayer and absorbing waveguides and are used throughout the further experimental investigations of EO materials described in further chapters.

4. Waveguide poling investigations

In this chapter an overview of the organic thin film poling methods is provided. Here also the author summarizes the results obtained during investigations of organic waveguide poling with corona triode**.**

4.1. Overview of NLO material types and poling methods

As was shown in section 2.5, the second order effects, such as EO and SHG effect, can only be observed in materials with intrinsic nonlinearity. Also, as noted, the macroscopic nonlinearity of material originates from the sum of microscopic or molecular nonlinearities.

The NLO organic materials can be classified into three major types depending on how the NLO molecules or the microscopic nonlinearities are incorporated in the material. The main NLO organic material types are molecular glasses, functionalized polymers and doped polymers [66].

Molecular glasses are formed of molecules consisting of multiple NLO chromophores in dendrimers, oligomers and other units. Theoretically, NLO active molecular glasses with high thermal stability could be obtained through structural modifications and thus are studied intensively. Appropriate structural modifications could introduce noncovalent intermolecular interactions such as hydrogen bonding or electrostatic interactions that would increase the glass transition temperature. However, it is hard to obtain high nonlinearity in molecular glasses mainly due to low orientational flexibility as well as aggregation of the large NLO molecules [131].

Alternatively, functionalized polymers could be used in the EO waveguide devices. In a functionalized polymer the NLO active molecule is incorporated either in the backbone or the side chain of the polymer [132,133]. In these materials, high concentration of the dopant, the NLO molecules, is allowed, as well as they demonstrate excellent thermal stability [134,135].

Historically, doped polymer materials were the first to be investigated. Such materials are also referred to as guest-host polymers. The NLO material consists of a polymer (host) which is doped by NLO chromophores (guest). Such polymer doping is the most straight-forward way for preparation of an NLO material. For some time the doped polymers lost their popularity, mainly due to poor success in the early stages of investigation of these materials. However, recently doped polymers have regained their popularity due to new understanding of molecular interactions in guest-host materials. New research results suggest that very high thermal stability and NLO efficiency could be obtained in a guest-host polymer [133,136].

With a few exceptions, organic NLO materials are originally centrosymmetric and require poling [133]. Poling is a process in which the macroscopic nonlinearity in the material is obtained by aligning the NLO molecules. The NLO molecules are aligned at temperatures above the material

glass temperature T_g. The alignment of the molecules is a result of dipolar interaction between the NLO chromophore and the electric field. After poling the molecule intrinsic alignment relaxation takes place [137]. This causes the nonlinearity of the material to decrease. The speed of relaxation depends on the glass transition temperature T_g of the material and the temperature at which it is used, as well as on the molecular interactions that may either sustain or reduce the noncentrosymmetricity of the material. It is important to note that the poling-induced order in the waveguide must be achieved without the introduction of surface damage or of material inhomogeneity, which may significantly increase the light propagation loss in the waveguide [138].

Material poling is one of the most important steps employed in the EO material preparation and in its investigation. For NLO organic material poling purposes multiple methods have been proposed in the literature.

The most straight-forward and simple waveguide poling approaches are the contact poling methods such as parallel-plate or in-plane poling methods [139]. In these methods the NLO material is placed between two conducting plates as shown in Fig. 4.1.A and Fig. 4.1.B, respectively. In the parallel-plate method, usually, the waveguide is prepared on a conducting surface and the top electrode is sputtered on top of the waveguide. During poling the polymer is heated up to the glass transition temperature T_g and the electric poling field E_p is applied between the parallel electrodes. In the in-plane method the electrodes are in one plane but separated by a gap. Both of these techniques are highly sensitive to the quality of the waveguide. A dielectric breakdown in the thin film may take place if the applied electric field exceeds the breakdown field which is usually dominated by point defects, such as dust particles in the material. In case of dielectric breakdown, the resistivity of the thin film reduces significantly. This means that the poling voltage drop over the poling area on the waveguide also decreases. Simply speaking, the current flows through the breakdown channel and the waveguide is not poled. To reduce the probability of dielectric breakdown in the NLO waveguide while poling with parallel-plane and in-plane methods, usually, buffer layers between the electrodes and the NLO material are introduced [140]. The influence of electrical properties of the buffer layers on NLO waveguide poling efficiency has been discussed in the article by Grote and colleagues [141].

NLO polymers can also be poled by the all-optical poling method. In this method, the material is illuminated with high intensity laser beams with light frequency ω and second-harmonic 2ω. The fundamental and second-harmonic beams interact with the NLO molecules and align them such that the material becomes noncentrosymmetric. This method has multiple advantages. It can be carried out at room temperature, it does not require additional electrodes, and micro-patterning can be introduced [142–144]. However, the implementation of the method can be quite cumbersome due to the fact that a phase-matching condition of the fundamental and second-harmonic beams in the material is required for maximal poling efficiency. Even though, the poling

efficiency is comparable to the materials poled in an electric field by parallel-plate method, the technique requires for the material resonance to be in the 2ω range [145]. This can limit the choice of materials which can be poled using the all-optical poling technique.

For material poling one can also use photo-assisted or photo-thermal poling (see Fig. 4.1.C). In both methods a laser beam is used while an electric field is applied. In photo-assisted poling the laser beam is used to excite the molecules [146,147]. During the electronic excitation and relaxation of the molecule, it changes its geometry or, in other words, geometric isomerization takes place. Due to such geometry variations the NLO molecule can alter its alignment and poling can be performed if an electric field is applied and the molecule possesses a dipole moment. Unfortunately, there are a limited number of material types that could be used for photo-assisted poling. In photo-thermal poling the laser beam is used for local heating of the material [148]. The molecules can move more freely where the temperature of the material is higher. Both of these methods can be used for micro-patterning of the NLO material.

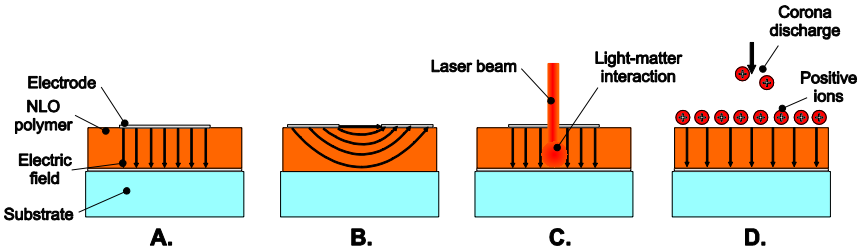

Fig. 4.1. NLO polymer waveguide poling methods. **A.** Parallel-plate poling method. **B.** In-plane poling method. **C.** Photo-assisted or photo-thermal poling. **D.** Corona poling. Corona discharge takes place near the corona needle.

Large nonlinearity in polymers can be obtained by electric poling with corona discharge [149–155]. The principles of this method are illustrated in Fig. 4.1.D. In this method the electric field in the material is created by ions which appear in the corona discharge process. This method is also referred to as the corona poling method. In an early study by Hill and colleagues it was shown that the corona poling is several times more effective than the contact poling methods, since higher poling voltages can be obtained [156]. This is mainly because even in case of local dielectric breakdown in the polymer during the corona poling, the voltage drop in the rest of the poling area does not occur due to low surface conductivity of the material. However, many research groups have indicated that surface and volume changes take place during poling [156–158]. Such changes cause the light propagation loss in the waveguide to increase significantly. The related investigations are still aimed toward finding the corona poling conditions at which the poling field would be

as high as possible and the optical quality of the waveguide would not be affected during poling.

4.2. Waveguide poling with corona triode

A simple corona poling can be performed by the two-electrode corona discharge setup as shown in Fig. 4.1.D [159]. The poling efficiency and controllability can be significantly increased if an additional electrode is introduced between the corona needle [160]. For waveguide poling investigations, the author of this thesis has used a computer controlled corona triode device. The device allows monitoring as well as controlling of the poling conditions. The particular corona triode setup as well as the influence of setup parameters on corona poling efficiency can be found elsewhere [160].

The NLO waveguide typical corona triode poling steps are shown in Fig. 4.2. During the corona poling, high voltage is applied to corona needle. By varying grid voltage, it is possible to control the polymer poling voltage. The voltage difference between the corona needle and the grid was kept constant of 9 kV to ensure invariable corona discharge conditions at different grid voltages. The ambient air in corona chamber was replaced by nitrogen to keep the corona generated ionic composition and conductivity independent of temperature and moisture. During the poling procedure the sample was put on a heater with precisely controlled temperature. Additional spacers between the grid and the sample could be introduced and thus the grid to sample distance could be varied.

The author of this thesis took part in the investigations devoted to increasing the poling efficiency of the NLO waveguides using the corona poling technique. These investigations are profoundly described in the article [P5].

During the first corona poling experiments it was recognized that the observable nonlinearity of the waveguide was low. The reduction of the observable nonlinearity was caused by the surface and/or spatial irregularities, which had appeared during poling. The optical microscope images of the unpoled and poled regions of PMMA+DMABI 10%wt thin waveguide which was poled by steps described above (caption of Fig. 4.2), are shown in Fig. 4.3.A and Fig. 4.3.B. Such inhomogeneity was observed in various NLO guest-host materials.

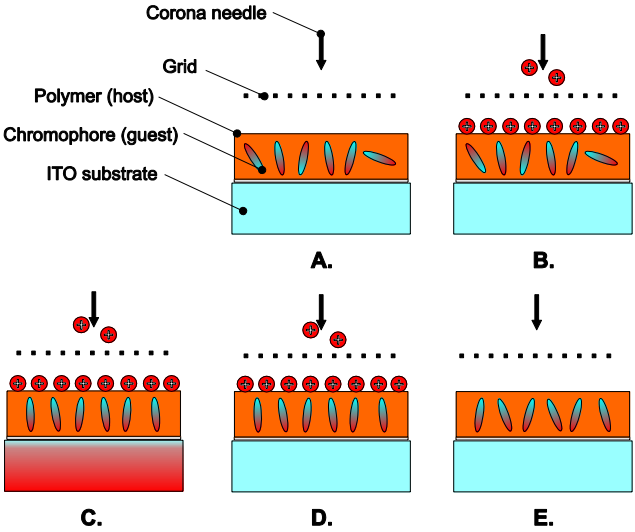

Fig. 4.2. The typical corona triode poling procedure. **A.** The polymer waveguide is initially centrosymmetric. The sample is placed into the corona triode device. **B.** Positive high voltage is applied to the corona needle and the grid. Positive ions are created as a result of corona discharge, and accelerated towards the surface of the waveguide. Ions on the surface of the sample create an electric field in the material. **C.** The sample is heated up to the poling temperature which is usually around the glass transition temperature T_g of the material. The temperature and high voltage on the needle and grid is sustained during the poling for a specific amount of time referred to as the poling time. **D.** The sample is cooled down to the ambient temperature. **E.** The high voltage is removed. The sample nonlinearity reduces slightly due to relaxation intrinsic alignment.

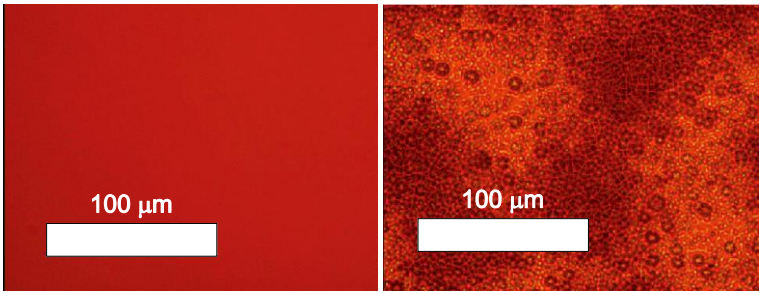

Fig. 4.3. Optical images of **A.** unpoled and **B.** poled regions of a PMMA+DMABI (10%wt) waveguide.

The extent of the inhomogeneity was characterized by measuring the scattered light intensity. It was found that the scattered light intensity depends on the poling electric field strength and the poling temperature, or on the ratio of poling and thermal energies, as well as on the distance between the sample and the grid.

During the investigations two main objectives were set. Firstly, it was necessary to understand and explain the reasons for the formation of inhomogeneity in the guest-host films during poling. The second objective was to find the optimal poling parameters at which the observable NLO efficiency of the material would be the highest.

To reach the first objective, the poled waveguides were extensively studied using optical, second harmonic (SH) and electron (SEM) microscopy. The optical images of the poled and light scattering area of the waveguide gave unclear understanding about the properties and the structure of individual scattering elements. Inspired by the results of recent theoretical calculations [161], a hypothesis suggesting formation of highly nonlinear molecular chains during the poling was proposed. The formation of such molecular chains in guest-host materials could enable the development of thermally very stable and highly nonlinear materials.

The SEM images of the inhomogeneity revealed a "hilly" structure of the waveguide surface, with the typical "hill" to "hollow" height differences of about 0.4 μm which is close to the half of the waveguide thickness. An SEM image of the poled DMABI+PMMA 10%wt waveguide is shown in Fig. 4.4.

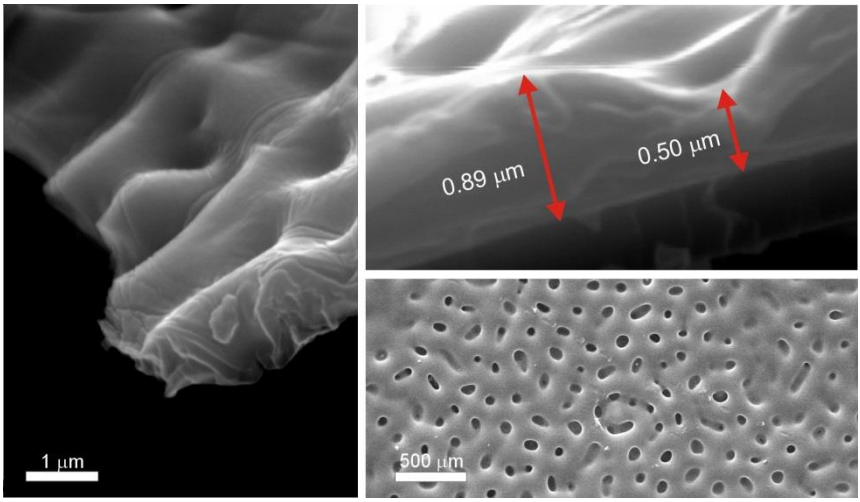

Fig. 4.4. An electron microscope image of the poled part of DMABI+PMMA 10%wt waveguide

The fact that the mass transport takes place in the waveguide during poling was also confirmed by two-photon excitation luminescence (TPL)

microscope measurements. The TPL and SH images of the hollow are shown in Fig. 4.5. Since the SH intensity characterizes the amount of noncentrosymmetric elements, the pattern in the SH image suggests that the chromophores (dipoles) are oriented towards or away from the hollow centers.

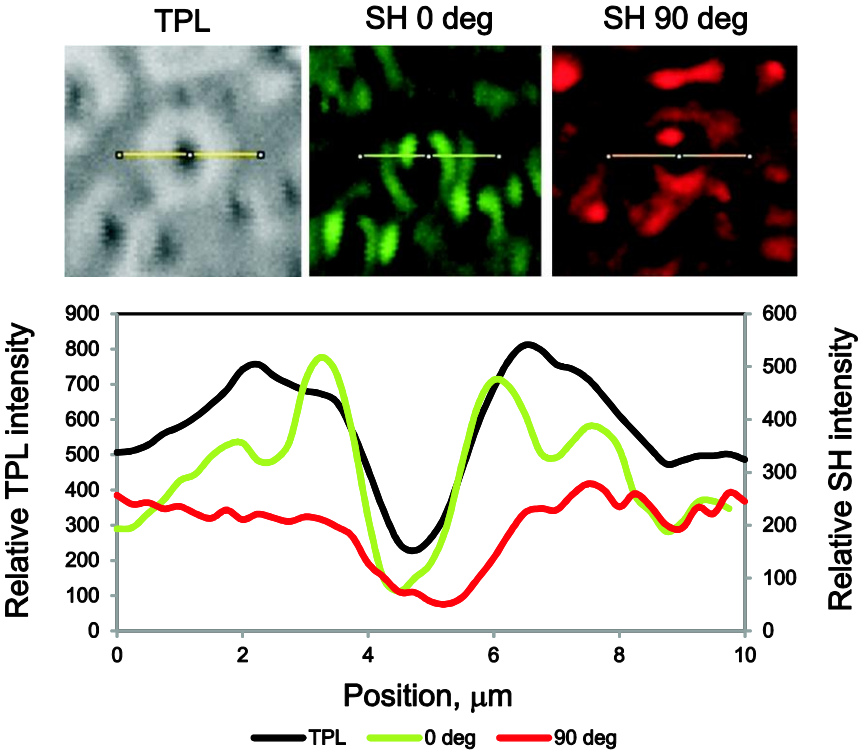

Fig. 4.5. TPL and SH intensities of the hollows scanned vertically after excited by ↔ polarized (0^o) and ↕ polarized (90^o) light.

Even though the used techniques for poled waveguide investigations allowed comprehending the structure of the inhomogeneity, the main driving force responsible for the mass transport in the waveguide during poling is still not fully understood. However, multiple hypotheses were put forward. The inhomogeneity in the form of hollows could be formed due to high energy ion bombardment [162]. During the investigations it was shown that the density of scattering elements or hollows grows if the kinetic energy of the ions is increased. This can be done either by increasing the grid voltage or decreasing the distance between the grid and the sample surface. However, in case nonpolar chromophores were dissolved in the host no changes in the sample morphology during the poling were observed. This result contradicts the

hypothesis that the mass transfer is caused by ion energy bombardment which should take place independently of the polarity of the molecules in the matrix. This also suggests that polar molecules are required in the thin film in order to observe formation of inhomogeneity. Thus possibly the changes in the sample morphology are induced by the poling field and chromophore dipole moment interaction which causes the mass transport to take place. The mentioned hollows could also be formed by local electrical breakdown in the film. This hypothesis is encouraged by the fact that a correlation could be observed between the sample conductivity and the probability for the changes in sample morphology to take place during the poling. Finally, a recent study suggests that hollows in the thin film that is subjected to a high electric field could be formed by bursting of solvent drops in the material [163]. This effect might also explain the experimental observations in the poled waveguides – the inhomogeneity is reduced if the sample is heated with no poling field applied. During this heating the solvent could leave the waveguide thus reducing the probability of bubble bursting.

The second objective – increasing of corona poling efficiency – was reached by changing the corona poling procedure. As mentioned previously, certain pre-poling steps helped to avoid formation of irregularities. This could be achieved by introducing film heating up to temperatures higher than the poling temperature for a short period of time with no poling field applied. Such approach helped to suppress the formation of an inhomogeneity for guest-host waveguide and increased the observable NLO efficiency.

4.3. Waveguide poling investigations: Summary

The corona poling method can be used for waveguide poling purposes. It, hypothetically, would allow wide area high electric field poling without being effected by local dielectric breakdown in the waveguide. However, as the poling fields are increased, surface and volume changes take place in the waveguide, causing the observable NLO efficiency to decrease and the optical propagation loss in the waveguide to increase. During the corona poling investigations, it was demonstrated that mass transport takes place in the waveguide. The origin of the mass transport phenomena is still not fully understood. Multiple hypotheses were put forward and discussed based on the obtained experimental results. Along with the mentioned discussions, certain poling parameters are suggested in [P5] for maximal poling efficiency with the corona poling technique.

5. Material nonlinearity investigations

After material poling, nonlinearity of the material has to be determined. Material nonlinearity is usually characterized by NLO coefficients and EO coefficients. The author of this thesis has implemented three techniques used for determination of thin film EO coefficients and has reported the results in four papers [P1,P2,P4,P8]. The paper [P8] holds the results of all of the implemented methods: Mach-Zehnder interferometric (MZI) technique, the Teng-Man ellipsometric (TM) technique and the attenuated total reflection (ATR) technique. None of the available techniques has yet been established as the standard for the determination of EO coefficients. Moreover, the major drawbacks of the techniques are not clearly outlined in the literature. As found by the author, incorrect interpretation of the measured experimental can lead to significant errors in the estimated material nonlinearity.

Before discussing the experimental results obtained during the implementation of the mentioned methods, the relevant theory is briefly presented. It should be complementary to the theoretical background provided in section 2 as well as in papers [P1,P2,P4,P8].

5.1. Derivation of EO coefficients

As shown in section 2.6. the EO effect is responsible for the change of the material refractive index with applied electric field. In order to comprehend how the EO coefficients influence the change of the refractive index, it is first valid to agree on the principal axis and the geometry. Usually, during the poling and EO measurements the electric field is applied parallel to the ***z*** axis according to the geometry evident in Fig. 5.1.

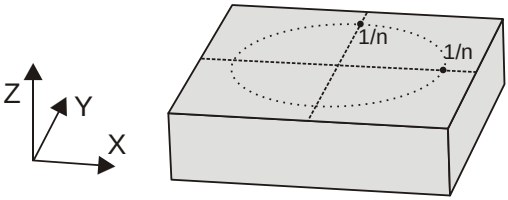

Fig. 5.1. The principal axes of the sample.

For retrieving the refractive index change as a function of the EO coefficients and the applied electric field, an index ellipsoid is used [85]. The index ellipsoid can be written as

$$\left(\frac{1}{n^2}\right)_1 x^2 + \left(\frac{1}{n^2}\right)_2 y^2 + \left(\frac{1}{n^2}\right)_3 z^2 = 1. \qquad (5.1)$$

The cross-section of the refractive index ellipsoid in the ***xy*** plane is also shown in Fig. 5.1.

The EO effect causes the ellipsoid surface to change, which can be estimated using (2.21) and (5.1) such that

$$\left(\frac{1}{n^2}\right)_1 x^2 + \left(\frac{1}{n^2}\right)_2 y^2 + \left(\frac{1}{n^2}\right)_3 z^2 + r_{13}E_z x^2 + r_{13}E_y y^2 + r_{33}E_z z^2 + 2r_{13}E_y yz^2 + 2r_{33}E_x xz^2 = 1. \quad (5.2)$$

Assuming that without the applied electric field we have zero birefringence in the sample, which is usually observed in weakly poled thin organic films [164], and that the electric field components $\boldsymbol{E_x}$ and $\boldsymbol{E_y}$ are zero, it is possible to obtain that

$$\left(\frac{1+n^2 r_{13}E_z}{n^2}\right)x^2 + \left(\frac{1+n^2 r_{13}E_z}{n^2}\right)y^2 + \left(\frac{1+n^2 r_{33}E_z}{n^2}\right)z^2 = 1. \quad (5.3)$$

The equation (5.3) gives the following new refractive indices:

$$n_x = \sqrt{\frac{n^2}{1+n^2 r_{13}E_z}}, \quad (5.4a)$$

$$n_y = \sqrt{\frac{n^2}{1+n^2 r_{13}E_z}}, \quad (5.4b)$$

$$n_z = \sqrt{\frac{n^2}{1+n^2 r_{33}E_z}}, \quad (5.4c)$$

Usually the refractive index change is small thus it is valid to assume that $\boldsymbol{r_{33}E_z}$<<1, which gives the refractive indices:

$$n_x = n - \frac{1}{2}n^2 r_{13}E_z, \quad (5.5a)$$

$$n_y = n - \frac{1}{2}n^2 r_{13}E_z, \quad (5.5b)$$

$$n_z = n - \frac{1}{2}n^2 r_{33}E_z, \quad (5.5c)$$

The equations (5.5a) through (5.5c) directly relate the refractive index of the material and the applied electric field intensity. If the refractive index change and the electric field intensities are known then the EO coefficient values can be calculated from the equations above.

It is important to note that the refractive index change is light polarization dependent. Let us assume that the incident light has the incidence plane parallel to the ***y*** axis. Then, in case the light is ***s*** polarized (perpendicular to the plane of incidence), the effective refractive change will be described by $\boldsymbol{r^s_{eff}}$, however, for the ***p*** polarized light (parallel to the plane of incidence) $\boldsymbol{r^p_{eff}}$ has to be used:

$$r^s_{eff} = r_{13}, \quad (5.6a)$$

$$r^p_{eff} = r_{13}cos^2\theta + r_{33}sin^2\theta, \quad (5.6b)$$

where $\boldsymbol{\theta}$ is the light propagation angle or the angle of refraction in the material.

5.2. Principles of EO modulated signal measurement

Multiple techniques have been used for the determination of EO coefficients [165–168]. Due to the fact that the refractive index change is very small (usually ~10^{-4}), almost all of the techniques employ an optical effect that is very sensitive to the refractive index change, such as interference or light coupling in the waveguide, as well as sensitive electronics that enable low electrical signal measurements.

The implemented MZI, TM and ATR techniques employ different optical phenomena for capturing the EO coefficient. However, in all of them the measurement of light intensity modulation depth is performed. The basic idea of EO coefficient measurement is shown in Fig. 5.2. In the MZI, TM and ATR optical setups a laser beam is used to probe the refractive index variations after the sample is subjected to a harmonic AC signal with a frequency ***f***. Due to the EO effect in the sample, changes in the light output of the optical setup can be observed. The output signal holds DC and AC components. The AC component with frequency ***f*** will be referred to as modulated signal. The amplitude of the modulated signal is very small and noisy. The lock-in (LI) amplifier detection technique is used to determine the amplitude of the modulated signal with a frequency ***f*** from the output signal [169]. In the LI amplifier the noisy output signal is multiplied with the AC reference signal giving the amplitude of the modulated signal. Any signal that is not of frequency ***f*** is strongly attenuated. The modulation depth in the context of this work is a parameter that characterizes the ratio of the amplitude of modulation signal and the DC signal from the detector. A detailed explanation of the measured parameters can be found in the papers by the author of this thesis [P4, P8].

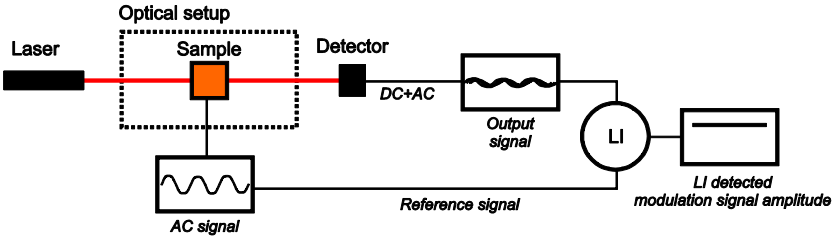

Fig. 5.2. The basic principles of LI detector based measurements. The output signal is electronically multiplied by the AC reference signal giving the amplitude of the modulation signal.

5.3. The MZI technique

Historically the MZI technique was the first to be implemented by the author. After reviewing the available literature on the subject of EO coefficient determination, the MZI technique was found to be the most simple and

sensitive of the techniques. Moreover, it allowed independent determination of both EO coefficients r_{13} and r_{33} if the modulation depth is measured at different light incidence angles on the sample.

The MZI technique is a two-beam interferometric setup. The first thin film EO coefficient measurements with the MZI technique were demonstrated in the early 80's [170,171]. In this technique the sample is put in one of the arms of the MZI. After the sample is subjected to an electric field, the light phase in the sample arm is changed causing the intensity at the output of the MZI to vary.

In the early stage of implementation of the MZI technique it was recognized that the technique is highly sensitive to mechanical vibrations. Also, the detected amplitude of the modulation signal held a considerable amount of cross-talk. This was an issue relevant also to other LI based measurements [P1]. Later it was demonstrated in papers [P2,P4,P8] that there are multiple other drawbacks of the technique that had not been sufficiently discussed in the literature. These drawbacks were related to the properties of the sample.

In the MZI technique transparent or semi-transparent electrodes in the samples are required. The first experiments were performed on sandwich type samples (see Fig. 3.2). The NLO organic material was placed between ITO coated substrates. The modulation voltage was applied on ITO electrodes. As noted in the Section 3 of this summary, an air gap forms between the surface of the EO polymer and the top ITO electrode. Moreover, light interference in the layers of the sample had a major influence on the modulated signal. When an AC voltage was applied to the electrodes, the air gap thickness varied causing the intensity modulations at the output of the MZI [P4]. The intensity modulations caused by the air gap thickness variations were at least an order higher than the EO modulations in the NLO thin film. The EO coefficients of the thin film could not be determined for such a sample design. To avoid formation of an air gap the electrodes were sputtered directly onto the thin EO active film. Such approach had several drawbacks – it was very likely to observe electrical breakdown in the samples, as well as the electrodes were highly absorbing. Also in such samples the multiple internal reflection (MR) effect could be observed. The MR effect significantly complicated the equations that could be used for characterization of the MZI data [172]. To account for the MR effects in the sample, an effective numeric approximation of the data based on Abelès matrix formalism was developed. The Abelès matrix formalism is a very powerful tool used for optical characterization of multilayer films [173,174] and waveguides [175,176]. The Abelès matrix formalism allows calculating the transmitted or reflected light intensity and phase. After the first approximations of the experimental data obtained by the MZI technique, it was found that the modulation amplitudes could not be described only by the EO effect. The data could be interpreted after the piezo- and electrostrictive thickness change (TC) effect was recognized to take place in the sample. The thickness of the thin polymer film was measured to vary

only on the order couple of tens of pm [P4]. However, the optical path length variations were comparable to the ones caused by the EO effect. Later theoretical analysis described in [P8] showed that the error that may appear in case of ignoring TC effect depends on the EO response of the sample. This error may be significant for the cases when the optical path length change due to the TC effect is comparable or greater than the optical path length change due to the EO effect. Therefore, it is always important to estimate the thickness variations of the sample before the EO coefficients of the film are determined.

5.4. The TM technique

In the TM setup, the EO effect caused phase variation between the orthogonally polarized components of the beam is registered. This method was independently introduced by Teng and Man [177] and by Schildkraut [178]. Currently it is one of most extensively used methods for the determination of EO coefficients.

The TM method is a very simple single-beam method which has low sensitivity to mechanical noise. For the implementation of the technique a variable light phase retarder is required. In the TM technique, the sample is operated in a reflection configuration. This means that only one of the electrodes in the sample has to be transparent. Based on the experience obtained during the implementation of the MZI method, the sputtered electrode was chosen to be the most suitable for the TM measurements. Similarly as in the MZI method, the MR effects also have to be considered when interpreting the TM measured data [178–180]. Unfortunately, the TC effect in relation with the TM measurements is barely discussed in the literature. Most authors assume a weak TC contribution in the measured signal [168,179].

For the TM measured data the numeric approximation of the data based on Abelès matrix formalism was implemented by the author. The principles of TM data approximation remained the same as for the MZI technique. In the code the changes in the characteristic equations were made accordingly. As demonstrated in [P8], the TM measured data interpretation based on Abelès matrix formalism showed to be surprisingly effective. Here all of the same considerations as in the MZI technique have to be applied when considering the influence of the MR and the TC effect. A simple analytic approximation of the data was also implemented for the EO modulation measurements that are performed at multiple incidence angles. The results of the TM measurements will be discussed in section 5.6.

5.5. The ATR technique

In the ATR technique the thin film waveguiding properties are exploited for the determination of EO coefficients [123,181,182]. This technique has some significant advantages over the TM and the MZI technique. It is inherently insensitive to the MR and has low sensitivity to TC effects in the

sample [165,168]. Due to this, the interpretation of the measured values is fairly straight-forward. Arguably the most complicated part of the technique is the preparation of suitable samples – the thin films must support guiding modes (see section 2.1), the film must be low-absorbing and have a low roughness surface.

The author of this thesis took part in the implementation of the technique which is profoundly described in the paper [P8]. The optical setup of the ATR method is very similar to the one used for light propagation loss measurements in the waveguides displayed in Fig. 3.5, with two differences. Firstly, for EO measurements the coupling point on the base of the prism has to be conducting to enable the application of an electric field. For this purpose a thin layer of gold (Au) was sputtered on the base of the prism. The slightly absorbing Au layer reduces the light coupling efficiency. Secondly, the light reflected from the prism's base facet is collected instead of the light that is coupled into the waveguide.

5.6. Comparison of the implemented techniques

The implemented techniques were compared via the EO measurement results of thin films. The corona triode device (see section 4.2) was used for poling purposes of the thin films. For all of the samples also the NLO coefficients were measured with the Maker fringe technique [111]. The NLO coefficient measurement can provide valuable information about the expected EO coefficients of the samples under investigation [91]. Therefore these measurements can introduce additional arguments about the validity of the implemented methods for determination of EO coefficients.

The measured EO coefficient r_{13} by the TM, MZI and ATR methods are evident in Fig. 5.3. Here the r_{13} is plotted against the measured NLO coefficient d_{31}. From Fig. 5.3 two significant features are obvious.

Firstly, the measured EO coefficients are smaller than estimated by the two-level model from NLO coefficient measurements. This could be due to overestimation of the r_{13}/d_{13} by the two-level model [168]. Secondly, it is evident that the coefficients measured by the ATR technique are by an order higher than the ones measured by the MZI or the TM technique. There could be several reasons why this could occur. Firstly, the samples that are used in the MZI and TM measurements could be actual modulating voltage could be smaller than expected in the TM and MZI measurements due to the capacitive nature of the sample – the sample could operate as a filter lowering the amplitude of the modulating electric field. This effect is not evident in the ATR method, since the capacity of sample is much smaller – the top electrode is only at the coupling point. Secondly, the sputtering of electrodes for the EO coefficient measurements may cause a local heating and depolarization of the polymer.

Along with EO coefficients measurements, the author performed an analysis of EO coefficient errors that may appear in the EO measurements due

to MR and TC effects. As is demonstrated in [P8] the MZI technique was the most sensitive to the TC effects. A surprising result was obtained by the TM method. If an angular scan of the modulated signal is performed, an analytic approximation that ignores MR and TC effects can provide an EO coefficient estimate with the precision within 2%. The retrieved EO coefficient values in the ATR method are much less sensitive to the TC effect. The error of estimated EO coefficient is low even if the TC caused modulations are several times higher than the EO modulations in the thin film.

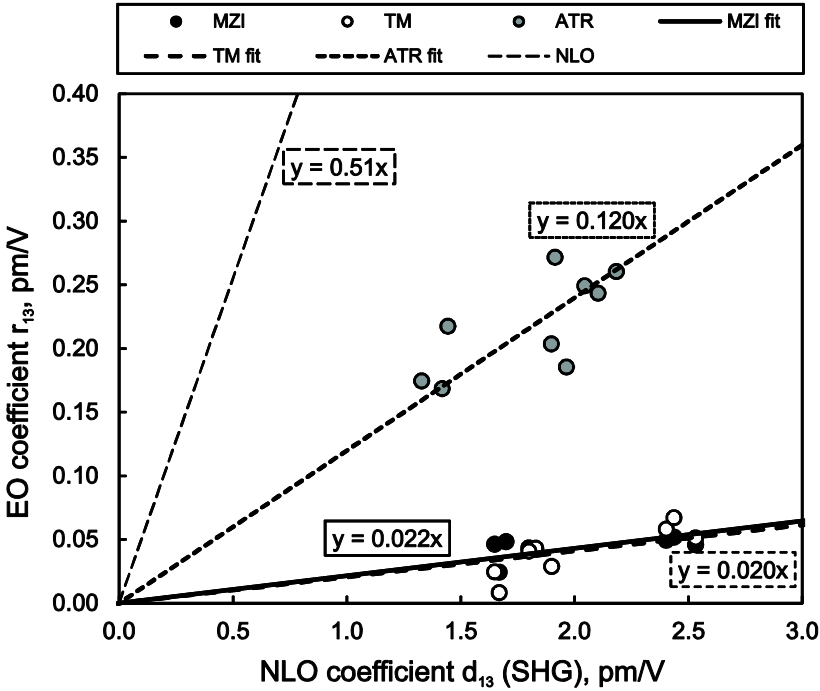

Fig. 5.3. The measured EO coefficient r_{13} as a function of measured NLO coefficient d_{13}: MZI, TM, ATR – r_{13} values measured by MZI, TM and ATR techniques, respectively; MZI fit, TM fit, ATR fit – a linear fit of the measured r_{13} values; NLO – a dashed line indicating the expected r_{13} as a function of d_{13} from the two-level model [91].

5.7. Material nonlinearity investigations: Summary

Three methods were implemented for the determination of EO coefficients for thin films. As was shown in the paragraphs above and in [P8], the techniques possess multiple advantages and drawbacks. Each of the implemented methods can be used for determination of EO coefficients of thin

films, however, the MR and TC effects multiple in the sample have to be considered. It was demonstrated that a numerical solution based on the Abelès matrix formalism can be used for the retrieval of the EO coefficient values from the experimental data obtained by MZI and TM methods. During the implementation of the methods it was recognized that the ATR is the most precise and simple technique for the determination of EO coefficients. This is mainly due to the fact that it has the least sensitivity to MR and TC effects.

6. Development of a hybrid SOI/polymer EO modulator

In the Introduction part of this work the author provided a brief overview of the current trends in the development of EO modulators. As noted, the organic materials are among the potential candidates to be applied as an EO medium in the modulator designs, mainly due to the advantageous properties such as low cost, easy processability, low dielectric constants and high nonlinearity. In this contribution the author has developed a new type of a SOI/polymer EO modulator design that could be capable of operating in the visible and IR range. The preparation steps as well as the performance parameters are briefly discussed in the following paragraphs. This chapter is based on the results that are profoundly described in the paper by the author and colleagues [P7].

6.1. Hybrid SOI/polymer waveguide design

The suggested hybrid SOI/polymer waveguide modulator comprises waveguides that are made on an SOI platform. Previously the SOI has been considered as a building platform for SP, which is justifiable – silicon is optically compatible with the communication wavelengths in the infra-red wavelength range. Only recently organic materials are being employed in the EO waveguide modulator designs on SOI, due to their very high optical nonlinearity.

The development steps of the invented waveguide structure are shown in Fig. 6.1 and described in the caption of the figure. The main preparation steps include etching a trench in the conducting silicon layer, oxidizing the silicon layer, and filling the oxidized trench with the EO polymer. The conducting silicon also serves as an electrode. This means that it can be used for in-situ polymer poling purposes as well as for EO modulation. The silicon oxide layer would serve as a waveguide cladding for the EO active waveguide core.

During the invention of the design, it was recognized that it possesses multiple very important advantages. Firstly, the preparation of the waveguiding element is very simple and cheap. Depending on the waveguide device, during the development of the waveguide only one lithography step may have to be employed. Secondly, the expected EO response of the NLO waveguide would be very high due to the fact that the modulation would take place in the NLO active waveguide core. Thirdly, the wavelength at which the designed waveguide may operate is limited only by the absorption of the used EO active organic material. Thus, by choosing an appropriate NLO material, the devices that employ the demonstrated waveguide design may operate over a wide range of electromagnetic spectra.

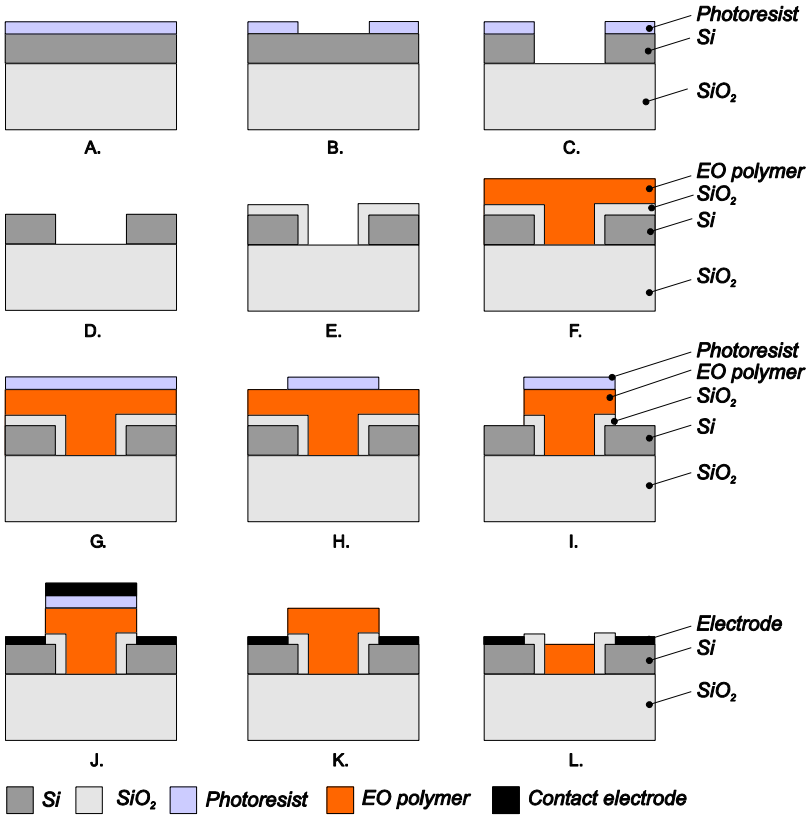

Fig. 6.1. Preparation steps of a hybrid SOI/polymer waveguide. **A.** A photoresist masking layer is applied on the SOI wafer. **B.-D.** Si layer is patterned using conventional lithography steps thus yielding a trench for further waveguide formation. **E.** The SiO_2 cladding layer is obtained by thermal oxidation of Si for a fixed period of time to obtain the required thickness of SiO_2 [183]. **F.** A ridge waveguide core is created in the formed trench by the spin coating or a blade casting of EO polymer [73]. **G.-I.** Additional photolithography steps are applied in order to remove the polymer and SiO_2 layers where contact metal electrodes will be applied (**J**). **K.** The photoresist layer is removed and, if necessary, the EO polymer thickness is reduced via etching (**L**). The step (**L**) is optional and could be applied in order to obtain a waveguide core with desired parameters.

The feasibility of the invented waveguide design was supported by theoretical simulations and experimental measurements [P7]. The greatest concern was that the visible light propagation loss in the waveguide could be very high due to the fact that the light would couple into high refractive index

silicon layers. The light out-coupling from the EO active core is determined by the thickness of the cladding layer as well as by the refractive indices of the EO core, the cladding and the silicon layer. Since the thermal oxidation limit for the oxide layer of decent quality on silicon is approximately 1 μm, the buffer layer will have to be less than the mentioned thickness. For experimental determination of light propagation loss in such waveguides, slab waveguides comprising an EO polymer core and an oxidized silicon cladding layer on silicon substrate were prepared. The measured propagation loss using travelling fiber method (see section 3) in a slab on oxidized silicon (SiO_2) substrate as a function of the oxide layer thickness is shown in Fig. 6.2. The experimentally measured propagation loss values are in good agreement with the ones obtained by numeric simulations. From the Fig. 6.2 it was concluded that the propagation loss in the waveguide would be dominated by the material properties if the oxidized silicon cladding layer was at least 0.75 μm thick.

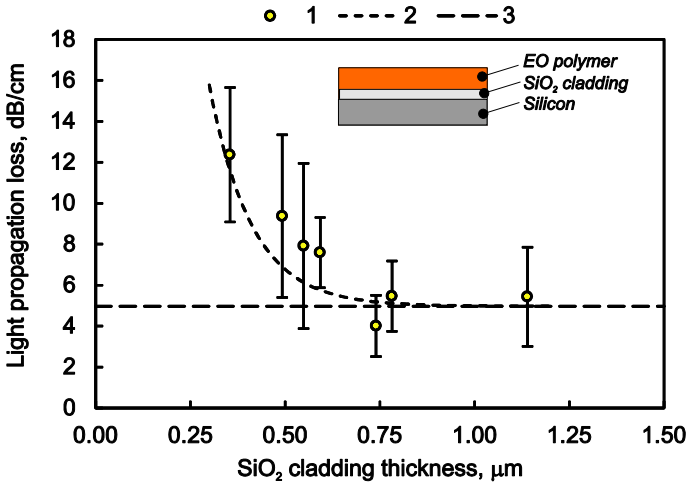

Fig. 6.2. Optical propagation loss of a slab waveguide consisting of DMABI-PSU 10 %wt as the waveguide core and a SiO_2 cladding layer which is on an absorbing high refractive index silicon substrate: 1 – experimental result; 2 – numerical result obtained by CAMFR; 3 – baseline corresponding only to the light propagation loss in the waveguide core due to light scattering and absorbance.

6.2. Hybrid SOI/polymer intensity modulator

As mentioned previously, the proposed preparation steps could be used for building active waveguide components such as a MZI type modulator. The cross-section and the top view of the suggested MZI SOI/polymer waveguide intensity modulator design are shown in Fig. 6.3.

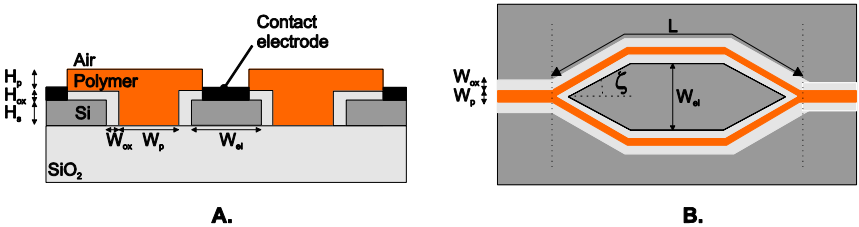

Fig. 6.3. A. The cross-section and **B.** the top view of the MZI SOI/polymer waveguide intensity modulator: W_p – polymer waveguide width, W_{el} – central Si electrode width, H_s – Si electrode height, W_{ox}=H_{ox} – SiO_2 cladding thickness, H_p – EO polymer thickness above the trench, L – length of the MZI modulator arm.

Several EO modulator optimization steps were conducted in order to understand the theoretical operational parameters [P7]. These mainly include optimization of geometrical parameters for low optical and control signals loss as well as for the highest EO efficiency. Some of the principal optimization steps are described briefly in the following paragraphs.

The MZI modulator design is optimized for low optical propagation and insertion loss. There are multiple effects that may cause the optical loss in the waveguide:

- intrinsic absorption – light is absorbed by the waveguide core and cladding materials;
- scattering loss – light is scattered at the rough boundaries of the waveguide;
- out-coupling loss during propagation – light is out-coupled from the core through the cladding into the substrate material. This can take place if **(i)** the first modes of waveguide are larger than the core and penetrate into the substrate or if **(ii)** the first modes get coupled into lower lossy modes due to the modal dispersion effect [69];
- bending loss – light is lost at bends or splits such as the Y-coupler of an MZI waveguide modulator;
- unpolarized light coupling loss – some part of the light is lost during coupling due to the fact that coupling conditions are met only for mode with specific polarization;

Besides the intrinsic absorption effect and scattering loss, which is dominated by the chosen waveguide materials and the waveguide preparation technique, the optical loss can be reduced significantly by optimizing the waveguide geometry. To reduce the probability of light coupling from waveguide core into the substrate, the cladding layer should be as thick as possible. Experimental measurements and numerical simulations confirm that the cladding has to be at least 0.75 μm thick in order to exclude the light

coupling into the substrate. This is considered in the further optimization of the modulator geometry. Also, the waveguide should operate in a single-mode operation regime in order to avoid the first modes being coupled into lower lossy modes. The waveguide dimension criteria were chosen as suggested in papers [184–187]. In the further steps the low birefringence regime was found. Essentially the main reason for optimization for low birefringence is the create conditions for high efficiency light coupling into the device. If the effective refractive indices are equal for the transfer electric and the transfer magnetic polarized light one should be able to couple both polarizations simultaneously, and, depending on the application, would not need to be concerned about the incoming light polarization.

The geometry of the modulator was also optimized for low bending loss which for an MZI modulator is governed by the splitting angle ζ in the Y-coupler (see Fig. 6.3 B). The splitting angle ζ will not only determine the light power coupled into the MZI arms, but also the size of the device. A lower splitting angle will require the modulator to be longer to achieve the optimal electrode width. It is therefore important to choose such splitting angle that will satisfy both the length and the optical loss requirements. The coupling efficiency in the Y-coupler as a function of the splitting angle ζ is shown in Fig. 6.4. As can be seen the loss increases significantly if the splitting angle ζ is higher than 10^o. Thus it is suggested to choose $\zeta < 10^o$.

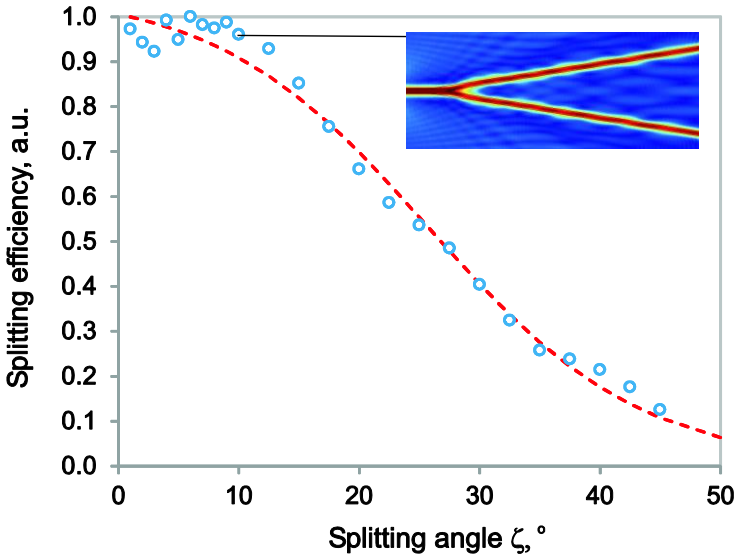

Fig. 6.4. The 2D numerically simulated optical splitting efficiency in the MZI Y-coupler as a function of the splitting angle ζ.

The EO modulator should also be optimized for high-speed operation. As noted in the Introduction part of this work, the MZI modulator has to be operated in a travelling-wave regime. In this regime the modulating electrical wave travels along with the optical wave in the waveguide causing EO modulation where the waves overlap. The loss of the modulation wave usually at GHz frequency depends on the geometry of the electrodes, dielectric constant and the resistivity of the electrode as well as on the dielectric properties of the materials that are surrounding the electrodes in the MZI modulator. The high-speed operation of the MZI travelling-wave modulator was obtained through geometry optimization via the quasi static – transverse electromagnetic (TEM) approach described elsewhere [7,13,188,59].

By optimizing the modulator design parameters it was demonstrated in [P7] that it is theoretically possible to achieve a switching voltage of 1.56 V·cm and a bandwidth of 1.9 GHz for an MZI modulator with 0.5 cm long arms and an EO coefficient of 100 pm/V. These results indicated that the suggested EO waveguide modulator could not be used for ultra-high speed light modulation. However, such an active waveguide structure and preparation technology could find its applications for making light switches, array waveguides for dense wavelength division multiplexing etc.

6.3. Development of a hybrid SOI/polymer EO modulator: Summary

The author has demonstrated the feasibility of a new type of hybrid SOI/polymer waveguide EO modulator. Theoretical calculations and experimental measurements conducted by the author confirm that the proposed EO modulator could operate both in the visible and the infrared wavelength range. The greatest benefit of the design is the simplicity of preparation and the high EO efficiency. It is important to note that the EO modulator design is currently pending an EU patent [Pa4].

7. Summary

The author of this thesis has discussed the results obtained during the implementation of methods for characterization of linear and non-linear optical properties of organic glass waveguides, waveguide poling investigations and the development of waveguide modulator design. This summary is a complementary part of the original articles by the author [P1-P8].

In the first chapters the author described three implemented methods for the characterization of the waveguide refractive index and thickness as well as the optical propagation loss in the optical waveguides. These methods are complementary and essential in the NLO characterization of organic materials and in the development of EO modulators.

Further chapter was devoted to the subject of EO waveguide poling which is a crucial part of an EO material preparation. In the poling studies the corona poling method was used. During the first corona poling experiments it was recognized that the observable nonlinearity of the waveguide was low. The reduction of the observable nonlinearity was caused by the surface and/or spatial irregularities, which had appeared during the poling process. This reduced the overall observable NLO efficiency of the films. During the poling investigations two main objectives were set and partly reached. Firstly, the increase of corona poling efficiency was achieved by addition of certain pre-poling steps in the waveguide preparation. A ten-fold increase in the NLO efficiency could be obtained. Secondly, the inhomogeneity was extensively studied using optical, second harmonic and electron microscopy. Even though, the origin of the mass transport phenomena was not fully understood, multiple hypotheses were put forward and discussed based on the obtained experimental results.

During the PhD studies, three methods for determination of EO coefficients for thin films were implemented. As was shown, each of the implemented methods can be used for determination of EO coefficients of thin films, however, the effects multiple internal reflection and thickness change in the sample have to be considered. It was demonstrated that a numerical solution based on the Abelès matrix formalism can be used for the retrieval of the EO coefficient values from the experimental data obtained by Mach-Zehnder interferometric and Teng-Man methods. The attenuated total reflection methods was recognized to be the most precise and simple for the determination of EO coefficients mainly due to the inherent sensitivity to the multiple internal reflection and thickness change effects.

In the final chapters, the author demonstrated a new type of hybrid SOI/polymer waveguide EO modulator. The feasibility and efficiency of the design was confirmed by numerical simulations and experimental measurements.

8. Main Theses

- The Abelès matrix formalism can be used for the retrieval of the electro-optic coefficient values from the experimental data obtained by Mach-Zehnder interferometric and Teng-Man methods.
- The multiple internal reflection and thickness change effects should be taken into account for correct determination of electro-optic coefficients from the experimental data obtained by Mach-Zehnder interferometric and Teng-Man methods.
- A hybrid silicon-on-insulator/polymer electro-optic waveguide modulator comprising electro-optic polymer as waveguide core, oxidized silicon as waveguide cladding and conducting silicon as electrode could be used for building passive and active electro-optic devices.

9. References

1. EC, "Towards 2020– Photonics Driving Economic Growth in Europe," http://www.photonics21.org/download/Brochures/Photonics_Roadmap_final_lowres.pdf.
2. F. P. Kapron, "RADIATION LOSSES IN GLASS OPTICAL WAVEGUIDES," Appl. Phys. Lett. **17**, 423 (1970).
3. Cisco, "Cisco Visual Networking Index: Forecast and Methodology, 2013–2018," http://www.cisco.com/c/en/us/solutions/collateral/service-provider/ip-ngn-ip-next-generation-network/white_paper_c11-481360.pdf.
4. S. Haykin, *Communication Systems*, 4th ed. (John Wiley & Sons, 2000), pp. 1–838.
5. J. Yamawaku, H. Takara, T. Ohara, K. Sato, A. Takada, T. Morioka, O. Tadanaga, H. Miyazawa, and M. Asobe, "Simultaneous 25 GHz-spaced DWDM wavelength conversion of 1.03 Tbit⁄s (103×10 Gbit⁄s) signals in PPLN waveguide," Electron. Lett. **39**, 1144 (2003).
6. Y. Miyagawa, T. Yamamoto, H. Masuda, M. Abe, H. Takahashi, and H. Takara, "Over-10 000-channel 2.5 GHz-spaced ultra-dense WDM light source," Electron. Lett. **42**, 655 (2006).
7. M. Minakata, "Recent Progress of 40 GHz high-speed LiNbO3 optical modulator," in *Proceedings of SPIE - The International Society for Optical Engineering*, A. K. Dutta, A. A. S. Awwal, N. K. Dutta, and K. Okamoto, eds. (2001), Vol. 4532, pp. 16–27.
8. M. Minakata, "LiNbO3 optical waveguide devices," Electron. Commun. Japan, Part II Electron. (English Transl. Denshi Tsushin Gakkai Ronbunshi) **77**, 37–51 (1994).
9. I. Suárez, P. L. Pernas, and G. Lifante, "Integrated electro-optic Mach–Zehnder modulator fabricated by vapour Zn-diffusion in LiNbO3," Microw. Opt. Technol. Lett. **49**, 1194–1196 (2007).
10. A. Melloni, F. Carniel, R. Costa, and M. Martinelli, "Determination of bend mode characteristics in dielectric waveguides," J. Light. Technol. **19**, 571–577 (2001).
11. E. L. Wooten, K. M. Kissa, A. Yi-Yan, E. J. Murphy, D. A. Lafaw, P. F. Hallemeier, D. Maack, D. V. Attanasio, D. J. Fritz, G. J. McBrien, and D. E. Bossi, "A review of lithium niobate modulators for fiber-optic communications systems," IEEE J. Sel. Top. Quantum Electron. **6**, 69–82 (2000).
12. T. Gorman and S. Haxha, "Design Optimization of Z-Cut Lithium Niobate Electrooptic Modulator With Profiled Metal Electrodes and Waveguides," J. Light. Technol. **25**, 3722–3729 (2007).
13. N. Anwar, S. S. A. Obayya, S. Haxha, C. Thernistos, B. M. A. Rahman, and K. T. V. Grattan, "The effect of fabrication parameters on a ridge Mach-Zehnder interferometric (MZI) modulator," J. Light. Technol. **20**, 854–861 (2002).
14. H. Chung, W. S. C. Chang, and E. L. Adler, "Modeling and optimization of traveling-wave LiNbO/sub 3/ interferometric modulators," IEEE J. Quantum Electron. **27**, 608–617 (1991).
15. H. Chung, W. S. C. Chang, and G. E. Betts, "Microwave properties of traveling-wave electrodes in LiNbO/sub 3/ electrooptic modulators," J. Light. Technol. **11**, 1274–1278 (1993).
16. K. Noguchi, O. Mitomi, K. Kawano, and M. Yanagibashi, "Highly efficient 40-GHz bandwidth Ti:LiNbO3 optical modulator employing ridge structure," IEEE Photonics Technol. Lett. **5**, 52–54 (1993).
17. L. N. Binh, "Lithium niobate optical modulators: Devices and applications," J. Cryst. Growth **288**, 180–187 (2006).
18. D. M. Gill, D. Jacobson, C. A. White, C. D. W. Jones, Y. Shi, W. J. Minford, and A. Harris, "Ridged LiNbO3 Modulators Fabricated by a Novel Oxygen-Ion Implant/Wet-Etch Technique," J. Light. Technol. **22**, 887–894 (2004).
19. G. K. Gopalakrishnan, W. K. Burns, R. W. McElhanon, C. H. Bulmer, and A. S. Greenblatt, "Performance and modeling of broadband LiNbO/sub 3/ traveling wave optical intensity modulators," J. Light. Technol. **12**, 1807–1819 (1994).

20. S. Haxha, B. M. A. Rahman, and K. T. V Grattan, "Bandwidth estimation for ultra-high-speed lithium niobate modulators," Appl. Opt. **42**, 2674–2682 (2003).
21. M. Koshiba, Y. Tsuji, and M. Nishio, "Finite-element modeling of broad-band traveling-wave optical modulators," IEEE Trans. Microw. Theory Tech. **47**, 1627–1633 (1999).
22. D.-G. Sun, Z. Liu, Y. Huang, S.-T. Ho, D. J. Towner, and B. W. Wessels, "Performance simulation for ferroelectric thin-film based waveguide electro-optic modulators," Opt. Commun. **255**, 319–330 (2005).
23. J. Leuthold, W. Freude, J.-M. Brosi, R. Baets, P. Dumon, I. Biaggio, M. L. Scimeca, F. Diederich, B. Frank, and C. Koos, "Silicon Organic Hybrid Technology—A Platform for Practical Nonlinear Optics," Proc. IEEE **97**, 1304–1316 (2009).
24. B. M. A. Rahman, V. Haxha, S. Haxha, and K. T. V Grattan, "Design optimization of polymer electrooptic modulators," J. Light. Technol. **24**, 3506–3513 (2006).
25. E. Nitiss, J. Busenbergs, and M. Rutkis, "Hybrid silicon on insulator/polymer electro-optical intensity modulator operating at 780 nm," J. Opt. Soc. Am. B **31**, 2446 (2014).
26. R. A. Soref and J. P. Lorenzo, "SINGLE-CRYSTAL SILICON: A NEW MATERIAL FOR 1. 3 AND 1. 6 mu m INTEGRATED-OPTICAL COMPONENTS.," Electron. Lett. **21**, 953–954 (1985).
27. W. Bogaerts, F. Martin, and D. Pieter, "Design Challenges in Silicon Photonics," IEEE J. Sel. Top. Quantum Electron. **20**, 8202008 (2014).
28. R. A. Soref and B. R. Bennett, "ELECTROOPTICAL EFFECTS IN SILICON.," IEEE J. Quantum Electron. **QE-23**, 123–129 (1987).
29. R. Soref, "The Past, Present, and Future of Silicon Photonics," IEEE J. Sel. Top. Quantum Electron. **12**, 1678–1687 (2006).
30. M. Oehme, K. Kostecki, M. Schmid, M. Kaschel, M. Gollhofer, K. Ye, D. Widmann, R. Koerner, S. Bechler, E. Kasper, and J. Schulze, "Franz-Keldysh effect in GeSn pin photodetectors," Appl. Phys. Lett. **104**, 161115 (2014).
31. Y.-H. Kuo, Y. K. Lee, Y. Ge, S. Ren, J. E. Roth, T. I. Kamins, D. A. B. Miller, and J. S. Harris, "Strong quantum-confined Stark effect in germanium quantum-well structures on silicon.," Nature **437**, 1334–6 (2005).
32. L. Alloatti, D. Korn, R. Palmer, D. Hillerkuss, J. Li, A. Barklund, R. Dinu, J. Wieland, M. Fournier, J. Fedeli, H. Yu, W. Bogaerts, P. Dumon, R. Baets, C. Koos, W. Freude, and J. Leuthold, "42.7 Gbit/s electro-optic modulator in silicon technology.," Opt. Express **19**, 11841–51 (2011).
33. M. Liu, X. Yin, E. Ulin-Avila, B. Geng, T. Zentgraf, L. Ju, F. Wang, and X. Zhang, "A graphene-based broadband optical modulator.," Nature **474**, 64–7 (2011).
34. B. Momeni, E. S. Hosseini, and A. Adibi, "Planar photonic crystal microspectrometers in silicon-nitride for the visible range.," Opt. Express **17**, 17060–9 (2009).
35. N. Horiuchi, "Nonlinear optics: Silicon nitride success," Nat. Photonics **6**, 412–412 (2012).
36. T. Ning, H. Pietarinen, O. Hyvärinen, J. Simonen, G. Genty, and M. Kauranen, "Strong second-harmonic generation in silicon nitride films," Appl. Phys. Lett. **100**, 161902 (2012).
37. K. Luke, A. Dutt, C. B. Poitras, and M. Lipson, "Overcoming Si_3N_4 film stress limitations for high quality factor ring resonators.," Opt. Express **21**, 22829–33 (2013).
38. J. P. Epping, M. Hoekman, R. Mateman, A. Leinse, R. G. Heideman, A. van Rees, P. J. M. van der Slot, C. J. Lee, and K.-J. Boller, "High confinement, high yield Si_3N_4 waveguides for nonlinear optical applications," Opt. Express **23**, 642 (2015).
39. L. R. Dalton, "Rational design of organic electro-optic materials," J. Phys. Condens. Matter **15**, R897–R934 (2003).
40. R. A. Norwood, C. Derose, Y. Enami, H. Gan, C. Greenlee, R. Himmelhuber, O. Kropachev, C. Loychik, D. Mathine, Y. Merzlyak, M. Fallahi, and N. Peyghambarian, "HYBRID SOL-GEL ELECTRO-OPTIC POLYMER MODULATORS: BEATING THE DRIVE VOLTAGE/LOSS TRADEOFF," J. Nonlinear Opt. Phys. Mater. **16**, 217–230 (2007).

41. D. M. Gill and A. Chowdhury, "Electro-optic polymer-based modulator design and performance for 40 Gb/s system applications," J. Light. Technol. **20**, 2145–2153 (2002).
42. B. A. Block, T. R. Younkin, P. S. Davids, M. R. Reshotko, P. Chang, B. M. Polishak, S. Huang, J. Luo, and A. K. Y. Jen, "Electro-optic polymer cladding ring resonator modulators," Opt. Express **16**, 18326 (2008).
43. L. Alloatti, D. Korn, C. Weimann, C. Koos, W. Freude, and J. Leuthold, "Second-order nonlinear silicon-organic hybrid waveguides.," Opt. Express **20**, 20506–15 (2012).
44. C. Gui and J. Wang, "Optical data exchange of m-QAM signals using a silicon-organic hybrid slot waveguide: proposal and simulation.," Opt. Express **22**, 24796–807 (2014).
45. T. Baehr-Jones, M. Hochberg, G. Wang, R. Lawson, Y. Liao, P. A. Sullivan, L. Dalton, A. K.-Y. Jen, and A. Scherer, "Optical modulation and detection in slotted Silicon waveguides," Opt. Express **13**, 5216 (2005).
46. C. Koos, P. Vorreau, P. Dumon, R. Baets, B. Esembeson, I. Biaggio, T. Michinobu, F. Diederich, W. Freude, and J. Leuthold, "Highly-nonlinear silicon photonics slot waveguide," in *Optics InfoBase Conference Papers* (Optical Society of America, 2008).
47. S. Xiao, Y. Li, Y. Hao, X. Jiang, and J. Yang, "High-speed compact silicon digital optical switch with slot structure," Opt. - Int. J. Light Electron Opt. **122**, 955–959 (2011).
48. J. Witzens, T. Baehr-Jones, and M. Hochberg, "Design of transmission line driven slot waveguide Mach-Zehnder interferometers and application to analog optical links.," Opt. Express **18**, 16902–28 (2010).
49. M. Gould, T. Baehr-Jones, R. Ding, S. Huang, J. Luo, A. K.-Y. Jen, J.-M. Fedeli, M. Fournier, and M. Hochberg, "Silicon-polymer hybrid slot waveguide ring-resonator modulator.," Opt. Express **19**, 3952–61 (2011).
50. I. E. Araci, R. Himmelhuber, C. T. DeRose, J. D. Luo, A. K.-Y. Jen, R. A. Norwood, and N. Peyghambarian, "Alignment-free fabrication of a hybrid electro-optic polymer/ion-exchange glass coplanar modulator.," Opt. Express **18**, 21038–46 (2010).
51. C. T. Derose, R. Himmelhuber, D. Mathine, R. A. Norwood, J. Luo, A. K.-Y. Jen, and N. Peyghambarian, "High Δn strip-loaded electro-optic polymer waveguide modulator with low insertion loss," Opt. Express **17**, 3316 (2009).
52. C. T. DeRose, D. Mathine, Y. Enami, R. A. Norwood, J. Luo, A. K.-Y. Jen, and N. Peyghambarian, "Electrooptic Polymer Modulator With Single-Mode to Multimode Waveguide Transitions," IEEE Photonics Technol. Lett. **20**, 1051–1053 (2008).
53. Y. Enami, C. T. DeRose, C. Loychik, D. Mathine, R. A. Norwood, J. Luo, A. K.-Y. Jen, and N. Peyghambarian, "Low half-wave voltage and high electro-optic effect in hybrid polymer/sol-gel waveguide modulators," Appl. Phys. Lett. **89**, 143506 (2006).
54. Y. Enami, D. Mathine, C. T. DeRose, R. A. Norwood, J. Luo, A. K.-Y. Jen, and N. Peyghambarian, "Hybrid cross-linkable polymer/sol-gel waveguide modulators with 0.65 V half wave voltage at 1550 nm," Appl. Phys. Lett. **91**, 093505 (2007).
55. H. Chen, B. Chen, D. Huang, D. Jin, J. D. Luo, A. K.-Y. Jen, and R. Dinu, "Broadband electro-optic polymer modulators with high electro-optic activity and low poling induced optical loss," Appl. Phys. Lett. **93**, 043507 (2008).
56. S.-K. Kim, W. Liu, Q. Pei, L. R. Dalton, and H. R. Fetterman, "Nonlinear intermodulation distortion suppression in coherent analog fiber optic link using electro-optic polymeric dual parallel Mach-Zehnder modulator.," Opt. Express **19**, 7865–71 (2011).
57. A. Leinse, M. B. J. Diemeer, A. Rousseau, and A. Driessen, "A novel high-speed polymeric EO Modulator based on a combination of a microring resonator and an MZI," IEEE Photonics Technol. Lett. **17**, 2074–2076 (2005).
58. B. Li, J. Vemagiri, and R. Dinu, "Design and Modeling of Traveling-Wave Electro-Optic Polymer Modulator for Ultrahigh Speed Applications," J. Light. Technol. **27**, 606–611 (2009).
59. K. Liang, Q. Song, F. Lu, B. Wu, W. Chen, H. Peng, C. Liu, and S. Luo, "Optimizing Design for the Traveling Wave Electrodes in Low-Drive High-Speed Electro-Optic Polymer Modulators," Fiber Integr. Opt. **24**, 521–528 (2005).

60. Z. Liu and D. Zhu, "A Low-loss Electro-optic Waveguide Polymer Modulator and its Optimization Design," Opt. Quantum Electron. **37**, 949–963 (2005).
61. H. Zhang, M.-C. Oh, A. Szep, W. H. Steier, C. Zhang, L. R. Dalton, H. Erlig, Y. Chang, D. H. Chang, and H. R. Fetterman, "Push–pull electro-optic polymer modulators with low half-wave voltage and low loss at both 1310 and 1550 nm," Appl. Phys. Lett. **78**, 3136 (2001).
62. S. Park, J. J. Ju, J. Y. Do, S. K. Park, and M. H. Lee, "Multi-channel electro-optic polymer modulator based on a novel side-chain polymer," in *Journal of Nonlinear Optical Physics and Materials* (2004), Vol. 13, pp. 329–334.
63. F. Yi, F. Ou, B. Liu, Y. Huang, S.-T. Ho, Y. Wang, J. Liu, T. J. Marks, S. Huang, J. Luo, A. K.-Y. Jen, R. Dinu, and D. Jin, "Electro-optic modulator with exceptional power-size performance enabled by transparent conducting electrodes.," Opt. Express **18**, 6779–96 (2010).
64. H. Erlig, B. Tsap, D. Chang, A. Szep, W. H. Steier, H. R. Fetterman, and L. R. Dalton, "Recent advances in electrooptic polymer modulators incorporating highly nonlinear chromophore," IEEE J. Sel. Top. Quantum Electron. **7**, 826–835 (2001).
65. Y. Shi, W. Lin, D. J. Olson, J. H. Bechtel, H. Zhang, W. H. Steier, C. Zhang, and L. R. Dalton, "Electro-optic polymer modulators with 0.8 V half-wave voltage," Appl. Phys. Lett. **77**, 1–3 (2000).
66. L. R. Dalton, D. Lao, B. C. Olbricht, S. Benight, D. H. Bale, J. A. Davies, T. Ewy, S. R. Hammond, and P. A. Sullivan, "Theory-inspired development of new nonlinear optical materials and their integration into silicon photonic circuits and devices," Opt. Mater. (Amst). **32**, 658–668 (2010).
67. Telcordia Technologies, "Generic Requirements for Passive Optical Components," http://telecom-info.telcordia.com/site-cgi/ido/docs.cgi?ID=SEARCH&DOCUMENT=GR-1209&.
68. F. Kajzar and J. Zyss, "Organic nonlinear optics: Historical survey and current trends," in *Nonlinear Optics Quantum Optics* (2012), Vol. 43, pp. 31–95.
69. C. Pollock, *Fundamentals of Optoelectronics* (Irwin Professional Publishing, 1995), p. 569.
70. X. Tong, *Advanced Materials for Integrated Optical Waveguides* (Springer International Publishing Switzerland, 2014), p. 552.
71. L. Chrostowski and M. Hochberg, *Silicon Photonics Design* (Wiley, 2013).
72. L. Chrostowski, J. Flueckiger, C. Lin, M. Hochberg, J. Pond, J. Klein, J. Ferguson, and C. Cone, "Design methodologies for silicon photonic integrated circuits," in *Proceedings of SPIE - The International Society for Optical Engineering*, L. A. Eldada, E.-H. Lee, and S. He, eds. (SPIE, 2014), Vol. 8989, p. 89890G.
73. T. Suhara, "Integrated Optics," in *Comprehensive Microsystems* (Oxford, 2007), pp. 165–200.
74. MARCATILI EAJ, "DIELECTRIC RECTANGULAR WAVEGUIDE AND DIRECTIONAL COUPLER FOR INTEGRATED OPTICS," Bell Syst. Tech J **48**, 2071–2102 (1969).
75. G. B. Hocker and W. K. Burns, "MODE DISPERSION IN DIFFUSED CHANNEL WAVEGUIDES BY THE EFFECTIVE INDEX METHOD.," Appl. Opt. **16**, 113–118 (1977).
76. M. Szpulak, W. Urbanczyk, E. Serebryannikov, A. Zheltikov, A. Hochman, Y. Leviatan, R. Kotynski, and K. Panajotov, "Comparison of different methods for rigorous modeling of photonic crystal fibers," Opt. Express **14**, 5699 (2006).
77. Z. Zhu and T. G. Brown, "Full-vectorial finite-difference analysis of microstructured optical fibers," Opt. Express **10**, 853–864 (2002).
78. Lumerical, "MODE Solutions," https://www.lumerical.com/tcad-products/mode/.
79. Comsol, "Comsol Multiphysics," http://www.comsol.com/comsol-multiphysics.
80. P. Bienstman, S. Selleri, L. Rosa, H. P. Uranus, W. C. L. Hopman, R. Costa, A. Melloni, L. C. Andreani, J. P. Hugonin, P. Lalanne, D. Pinto, S. S. A. Obayya, M. Dems, and K.

Panajotov, "Modelling leaky photonic wires: A mode solver comparison," Opt. Quantum Electron. **38**, 731–759 (2007).
81. D. F. G. Gallagher and T. P. Felici, "Eigenmode expansion methods for simulation of optical propagation in photonics: pros and cons," in *Proceedings of SPIE - The International Society for Optical Engineering*, Y. S. Sidorin and A. Tervonen, eds. (2003), Vol. 4987, pp. 69–82.
82. P. Bienstman and R. Baets, "Optical modelling of photonic crystals and VCSELs using eigenmode expansion and perfectly matched layers," Opt. Quantum Electron. **33**, 327–341 (2001).
83. Department of Information Technology at Ghent University, "CAMFR," http://camfr.sourceforge.net/.
84. T. Verbiest, K. Clays, and V. Rodriguez, *Second-Order Nonlinear Optical Characterization Techniques: An Introduction*, 1st ed. (Taylor & Francis Group, 2009), p. 192.
85. R. W. Boyd, *Nonlinear Optics*, 2nd ed. (Academic Press, 2003), p. 576.
86. D. M. Burland, R. D. Miller, and C. A. Walsh, "Second-order nonlinearity in poled-polymer systems," Chem. Rev. **94**, 31–75 (1994).
87. J. L. Casson, H.-L. Wang, J. B. Roberts, A. N. Parikh, J. M. Robinson, and M. S. Johal, "Kinetics and Interpenetration of Ionically Self-Assembled Dendrimer and PAZO Multilayers," J. Phys. Chem. B **106**, 1697–1702 (2002).
88. P. Damman, R. Vallée, M. Dosière, E. Toussaere, and J. Zyss, "Oriented crystallization of NLO organic materials," Synth. Met. **124**, 227–232 (2001).
89. M. G. Kuzyk, K. D. Singer, and G. I. Stegeman, "Theory of Molecular Nonlinear Optics," Adv. Opt. Photonics **5**, 4 (2013).
90. L. R. Dalton, A. W. Harper, and B. H. Robinson, "The role of London forces in defining noncentrosymmetric order of high dipole moment-high hyperpolarizability chromophores in electrically poled polymeric thin films," Proc. Natl. Acad. Sci. **94**, 4842–4847 (1997).
91. K. D. Singer, M. G. Kuzyk, and J. E. Sohn, "Second-order nonlinear-optical processes in orientationally ordered materials: relationship between molecular and macroscopic properties," J. Opt. Soc. Am. B **4**, 968–976 (1987).
92. R. E. Newnham, *Properties of Materials* (Oxford University Press, 205AD), p. 391.
93. R. H. Page, M. C. Jurich, B. Reck, A. Sen, R. J. Twieg, J. D. Swalen, G. C. Bjorklund, and C. G. Willson, "Electrochromic and optical waveguide studies of corona-poled electro-optic polymer films," J. Opt. Soc. Am. B **7**, 1239–1250 (1990).
94. C. Maertens, C. Detrembleur, P. Dubois, R. Jérôme, P.-A. Blanche, and P. C. Lemaire, "Synthesis and Electrooptic Properties of a New Chromophore Dispersed or Grafted in a Carbazolyl Methacrylate Matrix," Chem. Mater. **10**, 1010–1016 (1998).
95. O. Ahumada, C. Weder, P. Neuenschwander, U. W. Suter, and S. Herminghaus, "Electro-Optical Properties of Waveguides Based on a Main-Chain Nonlinear Optical Polyamide," Macromolecules **30**, 3256–3261 (1997).
96. W. N. Herman and L. M. Hayden, "Maker fringes revisited: second-harmonic generation from birefringent or absorbing materials," J. Opt. Soc. Am. B **12**, 416–427 (1995).
97. J. D. Swalen, "Review of organic thin films: Their characterizations and applications," in *American Chemical Society, Polymer Preprints, Division of Polymer Chemistry* (ACS, 1997), Vol. 38, pp. 930–931.
98. A. Franquet, J. De Laet, T. Schram, H. Terryn, V. Subramanian, W. J. van Ooij, and J. Vereecken, "Determination of the thickness of thin silane films on aluminium surfaces by means of spectroscopic ellipsometry," Thin Solid Films **384**, 37–45 (2001).
99. R. W. Collins, I. An, C. Chen, A. S. Ferlauto, and J. A. Zapien, "Advances in multichannel ellipsometric techniques for in-situ and real-time characterization of thin films," Thin Solid Films **469-470**, 38–46 (2004).
100. S. Costantino, O. E. Martínez, and J. R. Torga, "Wide band interferometry for thickness measurement," Opt. Express **11**, 952–957 (2003).
101. K. Etoh, "Determination method of optical properties," Appl. Opt. **34**, 159–162 (1995).

102. P. Hlubina, J. Luňáček, and D. Ciprian, "Maxima of the spectral reflectance ratio of polarized waves used to measure the thickness of a nonabsorbing thin film," Opt. Lasers Eng. **48**, 786–791 (2010).
103. M. Brindza, R. A. Flynn, J. S. Shirk, and G. Beadie, "Thin sample refractive index by transmission spectroscopy.," Opt. Express **22**, 28537–52 (2014).
104. R. D. L. KRONIG, "ON THE THEORY OF DISPERSION OF X-RAYS," J. Opt. Soc. Am. **12**, 547 (1926).
105. K. Lee, E. K. Miller, N. S. Sariciftci, J. C. Hummelen, F. Wudl, and A. J. Heeger, "Photoinduced absorption and photoinduced reflectance in conducting polymer/methanofullerene films: Nonlinear-optical changes in the complex index of refraction," Phys. Rev. B - Condens. Matter Mater. Phys. **54**, 10525–10529 (1996).
106. J. L. Musfeldt, D. B. Tanner, and A. J. Paine, "Method for the determination of the optical properties of highly conjugated pigments," J. Opt. Soc. Am. A Opt. Image Sci. Vis. **10**, 2648–2657 (1993).
107. K. Yamamoto and H. Ishida, "Kramers-Kronig analysis applied to reflection-absorption spectroscopy," Vib. Spectrosc. **15**, 27–36 (1997).
108. J. C. Manifacier, J. Gasiot, and J. P. Fillard, "A simple method for the determination of the optical constants n, k and the thickness of a weakly absorbing thin film," J. Phys. E. **9**, 1002–1004 (1976).
109. M. . Khashan and A. . El-Naggar, "A simple method of measuring and applying the dispersion of thin films," Opt. Commun. **187**, 39–47 (2001).
110. M. Bass, E. Van Stryland, D. Williams, and W. Wolfe, *Handbook of Optics*, 2nd ed. (McGraw - Hill, 1995), p. 832.
111. M. Rutkis, A. Vembris, V. Zauls, A. Tokmakovs, E. Fonavs, A. Jurgis, and V. Kampars, "Novel second-order non-linear optical polymer materials containing indandione derivatives as a chromophore," in *Organic Optoelectronics and Photonics II*, P. L. Heremans, M. Muccini, and E. A. Meulenkamp, eds. (2006), Vol. 6192, p. 61922Q–61922Q–8.
112. A. Savitzky and M. J. E. Golay, "Smoothing and differentiation of data by simplified least squares procedures," Anal. Chem. **36**, 1627–1639 (1964).
113. W. H. Press, B. P. Flannery, S. A. Teukolsky, and W. T. Vetterling, *Numerical Recipes in Fortran 77: The Art of Scientific Computing*, 2nd ed. (Cambridge University Press, 1992), p. 933.
114. V. Lucarini, K.-E. Peiponen, J. J. Saarinen, and E. M. Vartiainen, *Kramers-Kronig Relations in Optical Materials Research* (Springer-Verlag, 2005), p. 164.
115. F. W. King, "Efficient numerical approach to the evaluation of Kramers-Kronig transforms," J. Opt. Soc. Am. B Opt. Phys. **19**, 2427–2436 (2002).
116. F. W. King, "Numerical evaluation of truncated Kramers-Kronig transforms," J. Opt. Soc. Am. B Opt. Phys. **24**, 1589–1595 (2007).
117. G. E. Okecha, "Quadrature Formulae for Cauchy Principal Value Integrals of Oscillatory Kind," Math. Comput. **49**, 259–268 (1987).
118. K. Ohta and H. Ishida, "Comparison among several numerical integration methods for Kramers-Kronig transformation," Appl. Spectrosc. **42**, 952–957 (1988).
119. H. J. Trodahl, "Optical absorption in thin films," J. Phys. E. **17**, 27–29 (1984).
120. B. H. Robinson, L. R. Dalton, A. W. Harper, A. Ren, F. Wang, C. Zhang, G. Todorova, M. Lee, R. Aniszfeld, S. Garner, A. Chen, W. H. Steier, S. Houbrecht, A. Persoons, I. Ledoux, J. Zyss, and A. K. Y. Jen, "The molecular and supramolecular engineering of polymeric electro-optic materials," Chem. Phys. **245**, 35–50 (1999).
121. S. Zhu, Q. Fang, M. B. Yu, G. Q. Lo, and D. L. Kwong, "Propagation losses in undoped and n-doped polycrystalline silicon wire waveguides.," Opt. Express **17**, 20891–9 (2009).
122. T. N. Nguyen, K. Lengle, M. Thual, P. Rochard, M. Gay, L. Bramerie, S. Malaguti, G. Bellanca, S. D. Le, and T. Chartier, "Nondestructive method to measure coupling and propagation losses in optical guided structures," J. Opt. Soc. Am. B Opt. Phys. **29**, 3393–3397 (2012).

123. TIEN PK, "Light waves in thin films and integrated optics," Appl. Opt. **10**, 2395–2413 (1971).
124. Y. A. Vlasov and S. J. McNab, "Losses in single-mode silicon-on-insulator strip waveguides and bends," Opt. Express **12**, 1622 (2004).
125. S. Toyoda, N. Ooba, M. Hikita, T. Kurihara, and S. Imamura, "Propagation loss and birefringence properties around 1.55 μm of polymeric optical waveguides fabricated with cross-linked silicone," Thin Solid Films **370**, 311–314 (2000).
126. H. P. Weber, F. A. Dunn, and W. N. Leibolt, "LOSS MEASUREMENTS IN THIN-FILM OPTICAL WAVEGUIDES.," Appl. Opt. **12**, 755–757 (1973).
127. M. D. Himel and U. J. Gibson, "Measurement of planar waveguide losses using a coherent fiber bundle," Appl. Opt. **25**, 4413 (1986).
128. F. Wang, "Precision measurements for propagation properties of high-definition polymer waveguides by imaging of scattered light," Opt. Eng. **47**, 024602 (2008).
129. R. Ulrich and R. Torge, "Measurement of thin film parameters with a prism coupler.," Appl. Opt. **12**, 2901–8 (1973).
130. R. Fazludeen, S. Barai, P. K. Pattnaik, T. Srinivas, and A. Selvarajan, "A novel technique to measure the propagation loss of integrated optical waveguides," IEEE Photonics Technol. Lett. **17**, 360–362 (2005).
131. S.-H. Jang and A. K.-Y. Jen, "Electro-optic (E-O) molecular glasses.," Chem. Asian J. **4**, 20–31 (2009).
132. T. Aoyama, T. Wada, M. F. Beristain, and T. Ogawa, "Orientational Properties in Nonlinear Optical Polymers of Azo-Containing Poly(dipropargyloxybenzoates)," Mol. Cryst. Liq. Cryst. **446**, 55–60 (2006).
133. M. J. Cho, D. H. Choi, P. A. Sullivan, A. J. P. Akelaitis, and L. R. Dalton, "Recent progress in second-order nonlinear optical polymers and dendrimers," Prog. Polym. Sci. **33**, 1013–1058 (2008).
134. W. Shi, C. Fang, Y. Sui, J. Yin, Q. Pan, Q. Gu, D. Xu, H. Wei, H. Hu, and J. Yu, "Thermal stability and transmission losses of the poled polyimide side-chain thin films," Opt. Commun. **183**, 299–306 (2000).
135. J. Reyes-Esqueda, B. Darracq, J. García-Macedo, M. Canva, M. Blanchard-Desce, F. Chaput, K. Lahlil, J. . Boilot, A. Brun, and Y. Lévy, "Effect of chromophore–chromophore electrostatic interactions in the NLO response of functionalized organic–inorganic sol–gel materials," Opt. Commun. **198**, 207–215 (2001).
136. M. Rutkis, A. Jurgis, V. Kampars, A. Vembris, A. Tokmakovs, and V. Kokars, "New Figure of Merit for Tailoring Optimal Structure of the Second Order NLO Chromophore for Guest-Host Polymers," Mol. Cryst. Liq. Cryst. **485**, 903–914 (2008).
137. I. Rau, P. Armatys, P.-A. Chollet, F. Kajzar, Y. Bretonnière, and C. Andraud, "Aggregation: A new mechanism of relaxation of polar order in electro-optic polymers," Chem. Phys. Lett. **442**, 329–333 (2007).
138. L. Dalton, A. Harper, A. Ren, F. Wang, G. Todorova, J. Chen, C. Zhang, and M. Lee, "Polymeric electro-optic modulators: From chromophore design to integration with semiconductor very large scale integration electronics and silica fiber optics," Ind. Eng. Chem. Res. **38**, 8–33 (1999).
139. C. V. McLaughlin, X. Zheng, and L. M. Hayden, "Comparison of parallel-plate and in-plane poled polymer films for terahertz sensing," Appl. Opt. **46**, 6283 (2007).
140. R. Blum, M. Sprave, J. Sablotny, and M. Eich, "High-electric-field poling of nonlinear optical polymers," J. Opt. Soc. Am. B Opt. Phys. **15**, 318–328 (1998).
141. J. G. Grote, "Effect of conductivity and dielectric constant on the modulation voltage for optoelectronic devices based on nonlinear optical polymers," Opt. Eng. **40**, 2464 (2001).
142. Y. Wang, O. Y.-H. Tai, and C. H. Wang, "Second-harmonic generation in an optically poled azo-dye/polymer film.," J. Chem. Phys. **123**, 164704 (2005).
143. A. Apostoluk, J.-M. Nunzi, V. Boucher, A. Essahlaoui, R. Seveno, H. W. Gundel, C. Monnereau, E. Blart, and F. Odobel, "Permanent light-induced polar orientation via all-optical poling and photothermal cross-linking in a polymer thin film," Opt. Commun. **260**, 708–711 (2006).

144. C. Fiorini, F. Charra, and J.-M. Nunzi, "Six-wave mixing probe of light-induced second-harmonic generation: example of dye solutions," J. Opt. Soc. Am. B **11**, 2347 (1994).
145. C. Fiorini, J. M. Nunzi, F. Charra, F. Kajzar, M. Lequan, R. M. Lequan, and K. Chane-Ching, "Light-induced orientation of a low absorbing phosphine oxide azo-dye/PMMA copolymer: Towards a trade-off between transparency and photoinduced non-linearity," Chem. Phys. Lett. **271**, 335–340 (1997).
146. P. M. Blanchard and G. R. Mitchell, "Localized room temperature photo-induced poling of azo-dye-doped polymer films for second-order nonlinear optical phenomena," J. Phys. D. Appl. Phys. **26**, 500–503 (1993).
147. Y. Atassi, J. Chauvin, J. Delaire, J. F. Delouis, I. Fanton-Maltey, and K. Nakatani, "Reversible photoinduced modifications of polymers doped with photochromes : Anisotropy, photo-assisted poling and surface gratings," Mol. Cryst. Liq. Cryst. Sci. Technol. Sect. A Mol. Cryst. Liq. Cryst. **314**, 313–324 (1998).
148. H. Kobayashi, M. Kubo, T. Tsukada, and M. Hozawa, "Numerical analysis for photothermal poling process of nonlinear optical polymer film," Int. J. Heat Mass Transf. **45**, 865–875 (2002).
149. A. Hou, D. Zhang, K. Chen, and M. Yi, "Poling of organic polymer films for external electro-optic measurement," in *Symposium on Integrated Optoelectronics*, B. S. Dunn, E. J. A. Pope, H. K. Schmidt, and M. Yamane, eds. (International Society for Optics and Photonics, 2000), pp. 299–305.
150. J. M. Marshall, Q. Zhang, and R. W. Whatmore, "Corona poling of highly (001)/(100)-oriented lead zirconate titanate thin films," Thin Solid Films **516**, 4679–4684 (2008).
151. D. Möncke, G. Mountrichas, S. Pispas, E. I. Kamitsos, and V. Rodriguez, "SHG and orientation phenomena in chromophore DR1-containing polymer films," Photonics Nanostructures - Fundam. Appl. **9**, 119–124 (2011).
152. B. Yun, G. Hu, C. Lu, and Y. Cui, "Study on dipolar orientation and relaxation characteristics of guest–host polymers affected by corona poling parameters," Opt. Commun. **282**, 1793–1797 (2009).
153. J. A. Giacometti, S. Fedosov, and M. M. Costa, "Corona charging of polymers: Recent advances on constant current charging," Brazilian J. Phys. **29**, 269–279 (1999).
154. T. Fukuda, H. Matsuda, H. Someno, M. Kato, and H. Nakanishi, "Effective poling of high Tg NLO polymer," Mol. Cryst. Liq. Cryst. Sci. Technol. Sect. A Mol. Cryst. Liq. Cryst. **314**, (1998).
155. A. Vembris, M. Rutkis, and E. Laizane, "Influence of corona poling procedures on linear and non-linear optical properties of polymer materials containing indandione derivativatives as a cromophores," in *Proceedings of SPIE - The International Society for Optical Engineering*, P. L. Heremans, M. Muccini, and E. A. Meulenkamp, eds. (2008), Vol. 6999, pp. 699924–699924–6.
156. R. A. Hill, A. Knoesen, and M. A. Mortazavi, "Corona poling of nonlinear polymer thin films for electro-optic modulators," Appl. Phys. Lett. **65**, 1733 (1994).
157. Y. H. Min, K. S. Lee, C. S. Yoon, and L. M. Do, "Surface morphology study of corona-poled thin films derived from sol-gel processed organic-inorganic hybrid materials for photonics applications," J. Mater. Chem. **8**, 1225–1232 (1998).
158. S. M. Garner, V. Chuyanov, W. H. Steier, L. R. Dalton, A. Udupa, and H. R. Fetterman, "Optical intensity modulator based on a novel electrooptic polymer incorporating high mu beta chromophore," IEEE J. Quantum Electron. **36**, 527–532 (2000).
159. O. Vilitis, I. Muzikante, M. Rutkis, and A. Vembris, "Chromophore Poling in Thin Films of Organic Glasses. 2. Two-Electrode Corona Discharge Setup," Latv. J. Phys. Tech. Sci. **49**, 62–70 (2012).
160. O. Vilitis, E. Titavs, E. Nitiss, and M. Rutkis, "Chromophore Poling in Thin Films of Organic Glasses. 3. Setup for Corona Triode Discharge / Hromoforu Polarizēšana Plānās Organisko Stiklu Kārtiņās 3. Koronas Izlādes Triodes Ierīce," Latv. J. Phys. Tech. Sci. **50**, 66–75 (2013).
161. M. Rutkis and A. Jurgis, "Insight in NLO Polymer Material Behavior from Langevin Dynamic Modeling of Chromophore Poling," Integr. Ferroelectr. **123**, 53–65 (2011).

162. R. E. Lake, J. M. Pomeroy, H. Grube, and C. E. Sosolik, "Charge State Dependent Energy Deposition by Ion Impact," Phys. Rev. Lett. **107**, 063202 (2011).
163. Q. Wang, Z. Suo, and X. Zhao, "Bursting drops in solid dielectrics caused by high voltages.," Nat. Commun. **3**, 1157 (2012).
164. J. W. Wu, "Birefringent and electro-optic effects in poled polymer films: steady-state and transient properties," J. Opt. Soc. Am. B **8**, 142 (1991).
165. M. Dumont, Y. Levy, and D. Morichère, "Electrootpic organic waveguides: optical characterization," Org. Mol. Nonlinear Opt. Photonics **194**, 461–480 (1991).
166. M. J. Shin, H. R. Cho, J. H. Kim, S. H. Han, and J. W. Wu, "Optical Interferometric Measurement of the Electro-Optic Coefficient in Nonlinear Optical Polymer Films," J. Korean Phys. Soc. **31**, 99–103 (1997).
167. M. Aillerie, N. Théofanous, and M. D. Fontana, "Measurement of the electro-optic coefficients: description and comparison of the experimental techniques," Appl. Phys. B Lasers Opt. **70**, 317–334 (2000).
168. D. Morichère, P.-A. Chollet, W. Fleming, M. Jurich, B. A. Smith, and J. D. Swalen, "Electro-optic effects in two tolane side-chain nonlinear-optical polymers: comparison between measured coefficients and second-harmonic generation," J. Opt. Soc. Am. B **10**, 1894–1900 (1993).
169. P. Regtien, F. van der Heijden, M. Korsten, and W. Olthius, *Measurement Science for Engineers* (Elsevier, 2004), pp. 87–115.
170. M. Sigelle, "Determination of the electrooptic coefficients of 3-methyl 4-nitropyridine 1-oxide by an interferometric phase-modulation technique," J. Appl. Phys. **52**, 4199–4204 (1981).
171. K. D. Singer, M. G. Kuzyk, W. R. Holland, J. E. Sohn, S. J. Lalama, R. B. Comizzoli, H. E. Katz, and M. L. Schilling, "Electro-optic phase modulation and optical second-harmonic generation in corona-poled polymer films," Appl. Phys. Lett. **53**, 1800–1802 (1988).
172. F. Qui, X. Cheng, K. Misawa, and T. Kobayashi, "Multiple reflection correction in the determination of the complex electro-optic constant using a Mach-Zehnder interferometer," Chem. Phys. Lett. **266**, 153–160 (1997).
173. F. Abelès, "La détermination de l'indice et de l'épaisseur des couches minces transparentes," J. Phys. le Radium **11**, 310–314 (1950).
174. S. Larouche and L. Martinu, "OpenFilters: open-source software for the design, optimization, and synthesis of optical filters," Appl. Opt. **47**, C219–C230 (2008).
175. D. Rafizadeh and S.-T. Ho, "Numerical analysis of vectorial wave propagation in waveguides with arbitrary refractive index profiles," Opt. Commun. **141**, 17–20 (1997).
176. D.-G. Sun, Z. Liu, J. Ma, and S.-T. Ho, "Design and fabrication of electro-optic waveguides with self-assembled superlattice films," Opt. Laser Technol. **39**, 285–289 (2007).
177. C. C. Teng and H. T. Man, "Simple reflection technique for measuring the electro-optic coefficient of poled polymers," Appl. Phys. Lett. **56**, 1734–1736 (1990).
178. J. S. Schildkraut, "Determination of the electrooptic coefficient of a poled polymer film.," Appl. Opt. **29**, 2839–2841 (1990).
179. D. H. Park, C. H. Lee, and W. N. Herman, "Analysis of multiple reflection effects in reflective measurements of electro-optic coefficients of poled polymers in multilayer structures," Opt. Express **14**, 8866–8884 (2006).
180. Y. Levy, M. Dumont, E. Chastaing, P.-A. Chollet, G. Gadret, and F. Kajzar, "Reflection method for electrooptical coefficient determination in stratified thin film structure," Mol.Chryst.liq.Chryst.Sci.Technol. B **4**, 1–19 (1993).
181. S. Herminghaus, B. A. Smith, and J. D. Swalen, "Electro-optic coefficients in electric-field-poled polymer waveguides," J. Opt. Soc. Am. B **8**, 2311–2317 (1991).
182. W. H. G. Horsthuis and G. J. M. Krijnen, "Simple measuring method for electro-optic coefficients in poled polymer waveguides," Appl. Phys. Lett. **55**, 616–618 (1989).
183. B. E. Deal and A. S. Grove, "General Relationship for the Thermal Oxidation of Silicon," J. Appl. Phys. **36**, 3770 (1965).

184. A. G. Rickman, G. T. Reed, and F. Namavar, "Silicon-on-insulator optical rib waveguide loss and mode characteristics," J. Light. Technol. **12**, 1771–1776 (1994).
185. J. Schmidtchen, A. Splett, B. Schueppert, K. Petermann, and G. Burbach, "Low loss singlemode optical waveguides with large cross-section in silicon-on-insulator," Electron. Lett. **27**, 1486–1488 (1991).
186. L. Vivien, S. Laval, B. Dumont, S. Lardenois, A. Koster, and E. Cassan, "Polarization-independent single-mode rib waveguides on silicon-on-insulator for telecommunication wavelengths," Opt. Commun. **210**, 43–49 (2002).
187. S. P. Pogossian, L. Vescan, and A. Vonsovici, "The single-mode condition for semiconductor rib waveguides with large cross section," J. Light. Technol. **16**, 1851–1853 (1998).
188. E. J. Denlinger, "LOSSES OF MICROSTRIP LINES.," IEEE Trans. Microw. Theory Tech. **MTT-28**, 513–522 (1980).

Acknowledgements

The completion of this thesis would not have been possible without the input and support of many people.

First of all, I would like to express my deepest gratitude to my advisor Dr. Mārtiņš Rutkis, for the provided opportunity, guidance and encouragement throughout the work. His input in my professional and intellectual growth is invaluable.

The author also expresses gratitude to the colleagues at the ISSP, especially Dr. Oskars Vilītis, Jānis Busenbergs, Andrejs Tokmakovs, as well as to Prof. Vidmantas Gulbinas and Dr. Andrej Dementjev from the Center for Physical Sciences and Technology, who contributed greatly to the completion of this work. I also acknowledge the input from my former and current colleague students at the Laboratory of Organic Materials – Eduards Titavs, Rolands Usāns, Arturs Bundulis, Elza Liniņa – for their technical assistance. They made the important little things happen from which I benefited greatly. Special thanks to colleagues Dr. Linards Skuja and Kārlis Kundziņš at the ISSP for valuable discussions.

Finally, I would like to express the deepest gratitude to my family for their patience and tremendous support. My wife Julija, daughter Paula, and sister Dina, were my main source of joy and motivation.

This work has been supported by the European Social Fund within the project «Support for Doctoral Studies at University of Latvia».

ESF
EIROPAS SOCIĀLAIS FONDS

EIROPAS SAVIENĪBA
IEGULDĪJUMS TAVĀ NĀKOTNĒ

LATVIJAS UNIVERSITĀTE
ANNO 1919